Chapter 13
Efficient Visible-Light-Driven Perovskites Photocatalysis: Design, Modification and Application

Noor Haida Mohd Kaus, Mohd Lokman Ibrahim, Saifullahi Shehu Imam, Salma Izati Sinar Mashuri, and Yogesh Kumar

Abstract Perovskite-based photocatalysts are oxides with the general formula ABO_3 are interesting materials that remained essential in solving a great deal of energy and environmental remediation challenges. Recent key issues for high-efficiency solar or visible light photocatalysis are the effectiveness in rapid transport to the semiconductor surface and the separation of photo-generated electron-hole pairs; thus, substantial efforts have been made to design and develop new generation of perovskite-based photocatalyst systems to improve their possible use. The present article provides an up-to-date review of recent development of perovskites-and its related materials, including titanate-based, tantalite-based, niobium-based, ferrites and others, demonstrating a remarkably rapid development and promising results in photocatalytic performance particularly in visible light-driven applications. Furthermore, the review also includes modification strategies that are commonly employed to improve the photocatalytic performance of perovskites. Finally, the summary of recent developments of perovskites-based photocatalysis for viable applications.

N. H. Mohd Kaus (✉)
School of Chemical Sciences, Universiti Sains Malaysia, 11800 Penang, Malaysia
e-mail: noorhaida@usm.my

M. L. Ibrahim · S. I. S. Mashuri
School of Chemistry and Environment, Faculty of Applied Science, UiTM Shah Alam, Selangor, Malaysia
e-mail: mohdlokman@uitm.edu.my

S. S. Imam
Department of Pure and Industrial Chemistry, Bayero University, P.M.B 3011 Kano, Nigeria
e-mail: ssimam.chm@buk.edu.ng

Y. Kumar
Department of Physics, ARSD College, University of Delhi, New Delhi 110021, India
e-mail: ykumar@arsd.du.ac.in

S. Garg and A. Chandra (eds.), *Green Photocatalytic Semiconductors*,
Green Chemistry and Sustainable Technology,
https://doi.org/10.1007/978-3-030-77371-7_13

Keywords Perovskites · Photocatalysis · Material science · Visible-light · Water remediation · Semiconductor

13.1 Introduction

Visible-light-induced chemical transformations or photocatalytic is a procedure of significantly speed up reactions in the presence of a photocatalyst (single-electron redox mediator) which absorbs photon energy from light irradiation to generate photoinduced electrons and holes pairs. In particular, the photocatalysis transpire through single-electron pathways, utilizing visible-light response of organic reactions for the applications of wastewater treatment and environmental protection [12, 114, 163]. This procedure is environmentally and ecologically friendly, green and produced clean energy as opposed to conventional organic reactions [83]. The process particularly refers to heterogeneous photocatalysis that has remarkable interest nowadays and mainly focuses on perovskites semiconductors that possess distinctive electronic and optical properties, as well as the ability to photogenerated electron-hole pairs [24, 152] with higher stability and potential recyclability [42, 83, 183]. Mostly semiconductors with wide band gaps i.e. TiO_2, ZnO, etc. will restrict its applicability to ultraviolet (UV) wavelengths, reflecting just 5% of the universe's available solar light energy. Moreover, the rapid recombination of photogenerated electron-hole pairs results in a rapid dissemination of energy that decreases the performance of photocatalyst [89, 121].

Some conventional approaches to prevail over the drawbacks listed compasses the extension of the absorption to the spectrum of visible range [22, 86], and decreasing the recombination rate of the photogenerated electrons and holes [38, 156]. The solutions explored to boost photocatalytic performance include the construction of appropriate band gaps [77, 170], the employment of nanosized architechtures [183, 172, 174, 168], the implementation of interface design and facet-engineered surface [13, 52], utilization of dopants, as well as metal and non-metal co-catalysts [6, 95, 111], surface modification [54, 199] and the heterostructure construction [16, 189, 69, 101].

Amongst the most photocatalytic materials, perovskite-based catalytic (PCB) materials are auspicious photocatalytic materials with fascinating controllable physico-chemical and optoelectronic properties, such as electron mobility, redox performance, structural flexibility, efficient photocatalytic performance, long charge carrier lifetimes, excellent charge carrier mobilities, high absorbance coefficients, and uncomplicated bandgap engineering with facile fabrication route [126, 193, 194, 7, 106]. The complete replacement of cation A or B by other metals leads to variant interesting properties and alteration of the surface facets to create catalytic activity enhancement [73, 113, 127, 94]. As opposed to other visible-light active inorganic semiconductors, perovskite-type catalytic materials exhibited facile and effortless materials construction, application, and permit simple alteration of their semiconductor bandgap. In our study, we present a concise review to the current

findings and noteworthy properties of perovskite materials, accompanied by the enhancement techniques and their recent representative applications for improved photocatalytic properties.

13.2 Overview and Design of Perovskites-Based Photocatalysts

Perovskites are materials having similar crystalline unit cell as calcium titanate ($CaTiO_3$), that was first discovered by Aleksevich von Perovski in 1839 [18, 118]. They have general chemical formula ABX_3, where 'A' and 'B' are cations of different ionic radii (A larger than B), and 'X' which is a halogen or oxygen anion, holds 'A' and 'B' together through an ionic bond [44, 65, 191]. Such different anions and various cations form oxide perovskites and halide perovskites, both of which have BX_6 octahedra in their crystal structures, with 'A' cation located in the interstitial voids of the neighbouring octahedra (Fig. 13.1).

The catalytic activity of the perovskites is primarily attributed to the transition metal ion at the B-site, while their thermal endurance is mainly due to the rare earth ion at the A-site [5]. As a result of their photoelectric [141], luminescent [187], magnetic [9], and electrical properties [82], perovskites are used in the areas of biological imaging, ionic conductors, sensing, photocatalytic, electro-catalytic, information sensing and other numerous technological applications [191].

Among the perovskite materials, the perovskite oxide with the formula ABO_3 is a typical structure in inorganic chemistry [79]. It has demonstrated outstanding potential in the development of solid oxide fuel cells [207], solar cells [206], and ferroelectrics [40]. Various oxide perovskites such as titanates [109], ferrites [37], and tantalates [98] are photocatalytically active. The flexibility in the composition and structure of the oxide perovskites greatly influences their photocatalytic performance [143, 193, 194].

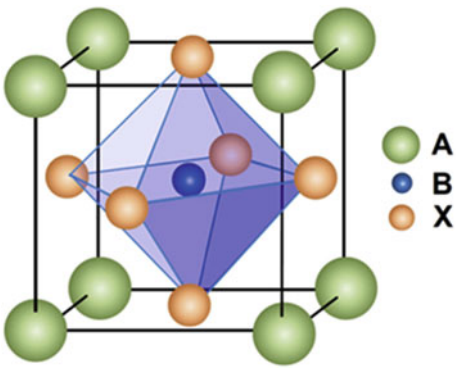

Fig. 13.1 ABX_3 perovskite unit cell (Reproduced with permission from Ref. [118])

Previously, perovskite materials were usually prepared using the traditional solid-state reaction method, but the produced materials are mostly heterogeneous, impure, have low light absorption in the visible region, are very sensitive to temperature changes, and the excited states have short lifetimes [2, 47]. To overcome these defects, alternative methods, including sol–gel [36], freeze-drying [88], combustion synthesis [92], electrospinning method [35], sonochemical method [110], coprecipitation method [81], microemulsion method [5], glycine-nitrate route [167] and microwave-assisted method [162] have been introduced. According to Tanaka and Misono [161], the main strategies of designing perovskite catalysts for the enhancement of their catalytic activity are; (1) selection of B-site elements which principally determine its catalytic activity, (2) valency and vacancy control by the selection of A-site elements, (3) synergistic effects of mainly B-site elements, (4) enhancement of surface area via formation of fine particles or dispersion on supports, and (5) addition of precious metals with their regeneration.

The efficiency of the catalyst, including perovskite materials during photocatalytic reactions, depends on three steps: (a) photon absorption and generation of charge carriers, (b) separation and transfer of charge carriers to the active sites of the surface, and (c) consumption of photogenerated charge carriers on the active sites during redox reaction [120]. Since most perovskites have a wide bandgap, several strategies have been employed to improve their visible light absorption and enhance the separation of photogenerated charge carriers. According to Moniruddin et al. [118], the key strategies include (a) bandgap engineering to achieve suitable band edge position, (b) enhancing the separation of charge carriers by changing particle size and crystal nanostructure, (c) improving visible absorption via the use of plasmonic metal nanoparticles (Ag or Au), (d) formation of heterojunctions to enhance separation of charge carriers, and (e) introduction of ferroelectric material to capitalize on its polarization field towards photoexcited charge separation. Specifically, various photo-active perovskites catalysts will be discussed in the following sub-sections.

13.2.1 Titanite Perovskites

One of the classified perovskite with general formula of $MTiO_3$ (M = Sr, Ba, Ca, Mn, Fe, Co, Ni, Pb, Cd) known as titanate perovskites [74]. They are promising photocatalysts with structural simplicity and flexibility [125]. Although most titanates are only active under UV light because of their wide bandgap, however, those containing transition metal oxides with d^0 and d^{10} orbitals, including Co^{2+}, Fe^{2+}, Ni^{2+}, Zn^{2+}, Pb^{2+}, and Cd^{2+}, would favour narrowing of the bandgap [21]. In general, titanates remain attractive materials in photocatalysis due to their high thermal stability and excellent resistance to photocorrosion [4, 100].

Among the titanate perovskites, $SrTiO_3$ happens to be the most widely studied titanate [164]. It is an n-type semiconductor posseseses an indirect bandgap between 3.1 and 3.7 eV, having a basic framework of Ti–O polyhedron as TiO_2,

and remarkable charge transport properties [47, 166, 200]. Furthermore, $SrTiO_3$ is cheap, less toxic, and easily doped to control its electrical properties [45, 173]. Although some narrow bandgap titanates such as $NiTiO_3$ (2.10 eV) and $CoTiO_3$ (2.28 eV) are visible light active, their conduction band is below the water oxidation potential. This limitation makes them unpopular [2]. Fortunately, despite its wide bandgap, the band edge for $SrTiO_3$ straddles the water splitting redox potential [74].

13.2.2 Tantalate Perovskites

Tantalates perovskites have the general formula $ATaO_3$ (A = Li, Na, K), and the bandgap of lithium, sodium and potassium tantalates was found to be 4.7, 4.0 and 3.6 eV, respectively [67, 122]. Although the tantalates are only active under UV light, however, they are interesting photocatalysts due to their good quantum yield, structural feasibility and environment-friendly nature [3, 41, 184]. Moreover, the respective Ta 5d orbital was placed at a negative site as compared to titanates. This could make the tantalates paramount during a photocatalytic reaction [15].

The high photocatalytic activity of tantalates has been related to their layered structure with a corner-shared framework of TaO_6, allowing easy transport and separation of photogenerated charge carriers [208]. $NaTaO_3$ is the most active tantalates perovskite [153], nevertheless it needs to be modified to extend their photodetection to the visible region to harness more solar energy [164].

13.2.3 Vanadate Perovskites

Vanadate perovskites have the general formula RVO_3 [177]. Among the vanadate perovskites, $AgVO_3$ is an efficient photocatalyst with favourable morphology and nanocrystalline nature [150]. It has two crystalline phases of α-$AgVO_3$ and β-$AgVO_3$, both of which have an intense absorption in the visible light region and are strongly dependent on temperature [50, 182]. At higher temperatures beyond 200 °C, α-$AgVO_3$ phase starts to convert into β-$AgVO_3$, and the process reaches completion at 300 °C [80]. Due to its more narrow bandgap, larger structural and chemical stability, β-$AgVO_3$ has gained more attention and wider application than α-$AgVO_3$ [81]. Although the CB potential of $AgVO_3$ is suitable for O_2 evolution and degradation of volatile organic compounds (VOCs), it is not sufficient for H_2 evolution [26].

13.2.4 Niobate Perovskites

Niobate perovskites can be identified as $ANbO_3$ (A = Na, K, Ag, Cu) [47]. Although they are only active under UV light due to their wide bandgaps (>3 eV), they can induce both photocatalytic water splitting and oxidative degradation of organic contaminants [208].

Among the niobate perovskites, sodium vanadate ($NaNbO_3$) and potassium vanadate ($KNbO_3$) are less toxic and environmentally friendly materials and have attracted considerable interest [56]. They are both indirect bandgap semiconductors, with $NaNbO_3$ having a bandgap of 3.4 eV, while $KNbO_3$ has a slightly narrow bandgap of 3.1 eV [78]. Band structure calculation revealed that the mobilities of both charge carriers are higher in $KNbO_3$ than in $NaNbO_3$ [151]. This, in addition to better light absorption, resulted in higher photocatalytic performance by $KNbO_3$ compared to $NaNbO_3$ [151].

13.2.5 Ferrite Perovskites

Ferrite perovskites have been identified as $AFeO_3$ (A = Bi, La, Gd, etc.), with their original bandgap in the visible area [74, 164]. Among the ferrite perovskites, $BiFeO_3$ photocatalyst is now parallel with the famous TiO_2-based photocatalysts [43]. Apart from its narrow bandgap, other interesting features of $BiFeO_3$ are non-toxic nature, high chemical stability, and the coexistence of ferromagnetic and ferroelectric behaviours at room temperature [64].

13.2.6 Bismuthate Perovskites

Bismuthate perovskites have the general formula $MBiO_3$ (M = Li, Na, K, Ag), and bandgap in the order $NaBiO_3$ (2.53 eV) > $KBiO_3$ (2.04 eV) > $LiBiO_3$ (1.63 eV) > $AgBiO_3$ (0.87 eV) [132, 159]. They consist of Bi^{5+} with 6 s empty orbital, contributing to both the valence band top and the conduction band bottom [204]. Such a feature can narrow the bandgap and vary the band edge positions, leading to improved photocatalytic performance [97, 96].

Despite the narrow bandgap of $AgBiO_3$, the large radius of Ag^+ and the strong contact between Ag atoms and O atoms hinders the free transfer of Ag^+ ions. However, due to small ionic radii of Li^+, Na^+, or K^+ and the weak interaction with [BiO_6] octahedrons, Li^+, Na^+, or K^+ ions may easily transfer in the tunnelled or layered space to harness solar energy [204].

13.2.7 Cobaltite Perovskites

Cobaltite perovskites have the general formula $ACoO_3$ (A = Gd, Sm, La, Pr, Eu, etc.) [51]. Among them, $LaCoO_3$ is considered as a promising catalytic material, as lanthanum (La) plays a vital role in the catalytic performance due to its partly occupied 4f levels [66, 115]. At the same time, the cobalt (Co) is considered active due to its mixed-valence state, excellent electrochemical behaviour, high electrical and ionic conductivities [49, 66]. However, partial visible light-harvesting ability, a short lifetime and recombination of photogenerated charge carriers limits its practical application [66].

13.2.8 Nickelate Perovskites

Nickelate perovskites have the general formula $RNiO_3$ (R = La, Pr, Nd, etc.), and $LaNiO_3$ has attracted considerable attention in multiple fields [63, 140]. As a result of its outstanding optoelectronic properties, inexpensiveness, suitable bandgap (1.9 eV) and non-toxic nature, $LaNiO_3$ has been deemed as an interesting and hopeful visible light photocatalyst for wastewater purification [188]. However, the conduction band position of $LaNiO_3$ is below the H^+/H_2 potential, and therefore electrons in the conduction band of $LaNiO_3$ could not be used for H_2 evolution [175].

13.2.9 Antimonate Perovskites

Antimonate perovskites have the general formula $ASbO_3$ (A = K, Ag, Cs, etc.), and $AgSbO_3$ has been reported as a promising material with positive response towards visible light [71]. The two main polymorphs of $AgSbO_3$ are the pyrochlore and ilmenite phases. The ilmenite $AgSbO_3$ phase was reported to show better photocatalytic performance towards the degradation of organic compounds under visible light irradiation than the pyrochlore $AgSbO_3$ phase [148]. However, the ilmenite $AgSbO_3$ phase is metastable and transforms into the stable pyrochlore $AgSbO_3$ phase by heat treatment under appropriate conditions [72].

The conduction band bottom of $AgSbO_3$ mainly consists of hybridized Ag 5 s and Sb 5 s orbitals, while the valence band top consists of hybridized Ag 4d and O 2p orbitals. The hybridization of orbitals leads to a continuous dispersion in a relatively wide energy range, resulting in high photocatalytic performance [90].

13.2.10 Chromite Perovskites

Chromite perovskites have the general formula $RCrO_3$ (R = La, Ce, Pr, Nd, Sm, Eu, Gd, Tb, etc.) [139]. Among the chromite perovskites, $LaCrO_3$ has been extensively examined due to its wide application in various fields, including photocatalysis [149]. It is a p-type visible light active perovskite photocatalyst with a bandgap of 2.6 eV [124]. The Cr-sites on the $LaCrO_3$ surface are better adsorption centres for atomic oxygen than Mn in $LaMnO_3$ or Fe in $LaFeO_3$ [169]. Such a feature in $LaCrO_3$ endows more favourable properties for photocatalytic applications [124].

13.2.11 Others

Apart from the above-discussed oxide perovskites, other oxide perovskites such as zirconates ($RZrO_3$ (R = Ca, Sr, and Ba)) [76], cerates ($RCeO_3$ (R = Ca, Sr, and Ba)) [28] and stannates [$RSnO_3$ (R = Ca, Sr, and Ba)] [201] also exists. However, they are barely used as photocatalysts, possibly due to their wide bandgaps [62, 70, 201].

13.3 Design and Modification Strategies

Solid-state technique is conventionally used to synthesize perovskites in the presence of basic salts at high thermal condition [39, 165]. Nevertheless, this method restricts the control of the particles dimension and its crystallinity [53]. On that account, an alternative method recently employed for the fabrications of tantalate perovskites, for instance, hydrothermal, [23, 25, 68, 84, 108]. solvothermal [29, 129] and polymerized complex method [178] to ensure the possibility of tuning the particle size with high surface area. It is interesting to note that, several modification strategies along with the alternative method are necessary to produce effective PCB with high photocatalytic performance. For example, the modification strategies particularly in defect engineering, doping and co-doping, sensitization, facet control and others.

The light absorption ability of the perovskite-based catalyst (PCB) was found to be enhanced when compared particularly with common wide band gap semiconductors (e.g., TiO_2), significant to the efficacy of photon and its carrier conversion. It is relevant to extend the duration of these carriers to further enhanced the photocatalytic performance. A befitting band gap is mostly crucial to optimize the absorption of light by the photocatalyst. Practically, the greater absorption in the visible range, the effectiveness of light absorption can be enhanced by tuning the band gap to be narrower [23, 25] The construction of the band structures is vital in

modulating the optical and electronic properties of perovskite nanostructures for achieving multifunctional the efficacy and efficiency [123].

In particular, the perovskite material has a direct band gap for the whole visible light range, therefore, the charge carriers were effectively generated at lower energies in particularly for photocatalytic application [123, 17]. Among all, PBC has been reported perspicuous approach for tuning the band gap, by simply adjusting the defects of crystal structure, including the vacancy, impurity and the interstitial atoms. It can be useful strategy for improving its performance [128, 197, 196] and lead to reduction in band gap value, thus improving the light absorption within visible range, subsequently possessed higher photocatalytic activity [10, 48].

13.4 Design and Modification Strategies

One of the internal influences that profoundly impact the performance of the photocatalyst is its configuration and modification in the physical structure and composition. To be an ideal photocatalyst, the material should have narrow band gap, high charge separation efficiency and a reasonable absorption efficiency under visible light. Many photocatalytic materials suffer from wide band gap energy which couldn't be stimulated by visible light (Zheng et al. 2015) and high recombination rate [57].

Conventional solid-state technique is commonly for synthesize perovskites perovskite materials at high temperatures [39, 165]. However, this approach limits regulation of crystallinity and particle size [53]. On that basis, for the manufacture of tantalate perovskites, hydrothermal technique currently used as an alternative strategy [23, 25, 29, 68, 84, 108, 129] and polymerized complex method [178] has been reported to ensure the possibility of tuning the particle size with better surface area. It is important to note that several modification strategies, along with the alternative method, are required to produce successful perovskite-based catalyst (PBC) with high photocatalytic efficiency. Several techniques have been developed to address these limitations, such as defect engineering, doping, heterojunction, sensitization, and other greener technique, i.e. integrated carbon-based material or biopolymers [111].

The light absorption ability of the perovskite-based catalyst was improved compared to typical large band gap semiconductors (e.g., TiO_2), as reported by Jiang and co-worker (2018). This improvement leading to the enhance the efficiency of photon to electron mobility. They proposed that it is important to increase the lifespan of these carriers to boost the overall performance of photocatalysts. An appropriate band gap is fundamentally crucial for optimizing the absorption of photocatalysts. In general, since the visible light range is greater, the absorption efficiency can also be enhanced by modulating the band gap to lower values [23, 25]. To achieve multifunctional efficacy and effectiveness, the engineering of band structures is crucial in tuning the optical properties and electronic states of perovskite nanostructures [123].

Some researcher reported the perovskite material has a direct band gap through the visible spectrum, so the charge carriers have been produced efficiently at lower energies, particularly for photocatalytic application [123, 17]. Relevant approach for tuning the band gap, by simply tuning the crystal structure defects, including the vacancy, impurity, and interstitial atoms, has been documented among the advanced features of different photocatalysts. According to [197, 196, 128], a proper tuning mechanism can be useful to enhance its efficiency and contribute to decreases in the value of the band gap, thereby increasing the light absorption in the visible spectrum and consequently allowing greater photocatalytic performance [10, 48].

13.4.1 Defect Engineering

The improvement in light absorption, catalytic efficiency, charge transfer and stability can be constructed by defect engineering. The defects were graded according to the defects and atomic structures of the semiconductor. In theory, structural discrepancies of photocatalysts can be classified into four such as point defects [146], line defects [131], planar defects [97, 96], and volume defects [99]. In addition, many photocatalysis with cation vacancies have been established by many researchers, and therefore significant to monitor the development of defects in perovskite materials by generating vacancies and self-doping.

For instance, one of the perovskites reported by Liu and Solhberg, [100] called strontium titanate, have been designed by defect engineering. $SrTiO_3$, a semiconductor of simple cubic and n-type with superior physical properties with bandgap between 3.1 and 3.3 eV. Despite the advantages, its wide optical bandgap restricts its capacity to absorb light, leaving most of the energy from solar light unused. Strategies to increase the photocatalytic potential of $SrTiO_3$ by controlling its bandgap to allow use of a wider visible and solar spectrum range. In this example, introducing defect or doping technique was done for the tuning of the $SrTiO_3$ bandgap.

Xie and co-workers [181] constructed self-doped $SrTiO_3$ through one-step combustion technique. The samples were treated with argon, Ti^{3+} ion vacancies and oxygen (O_2) were injected into the lattice, serving as a template to activate water molecules, helping to restore the efficacy of artificial photosynthesis. This study was able to show that these oxygen deficiencies are accommodated by inducing the gap that enables photoexcitation within the visible light region from the defect band to the conduction band, consequently encourage the adsorption for reduction of CO_2 under visible light irradiation.

In another study investigated by Luo et al. [107], they stated that the link between strontium titanate surface and its photocatalytic behaviour on CO_2 reduction. As reported, the surface of TiO_2-terminated surface is in low pH, so the electronic properties of the two Sr and Ti surfaces experienced significant different, where the Sr 4d orbital is more negative than the Ti 3d orbital in the conduction

band, resulting in greater SrO-terminated surface reduction potential. The study indicates that $SrTiO_3$ surface-Ti-rich had the greatest potential for reducing CO_2.

Kwak and Kang [87] have attempted to comprehend the effect of the Ca: Ti ratio towards $CaTiO_3$ and its potential efficiency. They reported a s the molar ratio of Ti in the catalyst extends up, a reaction between the reactive sites and carbon dioxide molecules occur. Nevertheless, it is reported that an excess of Ti will prohibit both metals from having a synergistic impact. $CaTiO_3$ encapsulated basalt fibre was recorded as an assisted material to create the highest numbers of oxygen vacancies on the planes {001} and sufficient pores size that allowed facilitating of CO_2 as indicated by Im et al. [61]. The fiber consisting of large amounts of SiO_2 with impurities of CaO, Al_2O3, and Fe_2O_3 [27] having a role as photosensitizer to enhance photocatalytic efficiency [30, 61].

In a separate approach, Hou et al. [55] disclosed the presence of nitrogen and oxygen vacancy are able to modulate the electronic bandgap NaTaON, thereby increasing the absorption of visible light. As these vacancies able to shifts the absorption of visible light from the UV region, resulting in a reduction in the 2.18 eV bandgap. The heterojunction also increased the separation of charged and improved the durability of the materials, thus improved the activity of CO_2 reduction.

13.4.2 Doping or Co-doping

Doping or co-doping, which is modulated by the inclusion of a foreign element in photocatalysts, is another alteration technique. Metal impurities are introduced into the lattice of perovskite as foreign atoms in the doping technique. Doping modifies the band gap and the material's atomic composition, thus making it possible to employ the visible light. In addition, Huang et al. [57] stated the additional energy levels can be added that help trap excitons in separate carriers while avoiding recombination. Many researchers utilized metallic elements and non- metallic elements doped perovskite [14, 102, 144, 192, 198] to modulate the band composition and electronic behaviour of studied photocatalysts.

The assortment of modifications has been investigated to broaden the photocatalyst bandgap and thus expand their photo-response to the visible light field, as reported by Samsudin and Abd Hamid [136] utilising noble metal deposition or known as doping. In other work, the significant observation by Anzai et al. [8] stated that the photocatalyst Ag-doped $CaTiO_3$ showed a higher generation rate and greater CO formation selectivity. In this study, Ag nanoparticles serve as unique active site within $CaTiO_3$ that reduced the production of H_2, and subsequently increased the creation of CO in water splitting.

Furthermore, by co-doping with La and Cr rare-earth metal, Wang et al. [172, 174, 168] successful modified hollow $CaTiO_3$ cubes to reduce the bandgap and boost their light-harvesting. In contrast to the small bandgap of pristine $CaTiO_3$, the hollow cubes exhibited stronger photocatalytic activity. This was primarily due to

the improved photon interactions in La/Cr co-doping as well as the shorter charge transport paths. Another series of La/Cr perovskite compounds co-doped with $ATiO_3$, of which A ¼ Ca, Sr and Ba were studied by Lu et al. [105] to see the differences in crystal structure as well as their optical and physicochemical properties. Critical structural contortions can be found for $Ca_{0.9}La_{0.1}Ti_{0.9}–Cr_{0.1}O_3$, indicating that Cr is responsible for the apparent light photoactivity. Lu et al. [105] discovered that the divergence away from the bond angle of Ti–O–Ti contributed to low catalytic efficiency as visible light absorption deteriorates. However, the existence of Ti–O–Ti bond angle ensures optimum overlap between Ti 3d orbitals and O 2p orbitals, resulting in broad band distribution and raised in charge movement for effective H_2 generations under visible light illumination.

Huang et al. [58] explored the properties of $BaTiO_3$ perovskite structure, by adjusting the concentrations of dopant elements such as selenium, tellurium and sulfur. These dopants substantially minimize the energy gap of $BaTiO_3$, thereby increasing absorption of the catalyst in the visible region. The catalytic properties of potassium tantalate, $KTaO_3$, studied by Chen et al. [23, 25] was doped with carbon and evaluated in the H_2 generation under sunlight illumination. From the observation, carbon-doped $KTaO_3$ demonstrated improved efficiency in the H_2 generation rate relative to the parent materials. In contrast, Krukowska et al. [84] investigated the role of lanthanides for $KTaO_3$-doped material and its efficiency towards generation of H_2. Synergistic results found between ion-doped perovskites of $KTaO_3$ and lanthanides and have strengthened the formation of H_2.

Depending on the crystallographic orientation, $BiFeO_3$ a perovskite oxide in rhombohedral unit cell and space group of *R3c* has known to be readily visible light active with a direct bandgap between 2.2 and 2.7 eV [138, 186]. In addition, doped or pristine ferrites materials are extensively studied in photocatalysis. For example, Yang and co-workers (2019) used Gd-doped $BiFeO_3$ as an efficient catalyst in generating H_2 in water splitting application. Meanwhile, Satar et al. [137] suggested that the band gap of $BiFeO_3$ decreased substantially in the presence of yttrium doped, increasing the percentage degradation of cationic dye, MB under sunlight irradiation. The authors claim, changes in performance are primarily due to electrons and holes being effectively produced, separated, and migrated.

13.4.3 Heterojunction

Heterojunction is another technique to improve the performance of the photocatalytic by increasing the efficiency of charge separation. Several studies conducted by Dutta et al. [33] and Ola and Maroto-Valer [121] showed, by bridging the semiconductor with metals or non-metals, heterostructures are produced that introduce new energy states that help to separate photogenerated charges and thereby preventing the electron from recombining. Ruzimuradov et al. [134], for instance, developed lanthanum- and N-co-doped strontium titanate-heterostructured

macroporous monolithic materials with a bi-continuous morphology of titanium dioxide in visible light-active condition.

A number of works reported [11, 75] based on the effect of p-type coupled with n-type materials to form a p–n heterojunction photocatalyst in addition to doping. In specific, the efficacy of CO_2 reduction in the presence of $BiFeO_3$–ZnO p–n heterojunction has been investigated by Karamian and Sharifnia [75]. The author reported that the composite showed higher optical responses in the visible light spectrum with higher performance in charge separation. This is largely due to the existence of the p–n heterojunction that has supplied the CO_2 photoconversion with an excess of energetic electrons.

In another study, Bagvand et al. [11] investigated the role of ZnS for the production of n-type photocatalyst of $BiFeO_3$ and its efficiency effect by controlling ZnS and ZnO molar ratios. The findings demonstrated the highest efficiency of photocatalytic CO_2 reduction at the equivalent molar ratio of both ZnO, ZnS and $BiFeO_3$ in the experiments. They claim that p–n structure will produce localized electrical field that contributes to the transition in the opposite direction of charge carriers, leading to a reduction of the recombination rate.

13.4.4 Sensitization and Facet Defect

Another strategy in crafting heterojunction for improved photocatalyst efficiency is facet engineering. Facet engineering is a potent approach to intensify the crystal's photocatalytic efficiency by inducing the creation of the facet defect by modulating the environment in which the crystal is being formed. The variation of surface energy of facets will affect the photocatalytic behaviour. There are several types of facets of the semiconductor lattice. Studies by Liu et al. [103] detected facets {110} and {101} possess low surface energy and stable, while the {001} facet has the greatest surface energy and highly reactive, respectively.

Interesting research finding by Yu et al. [190] has shown that {101} and {001} facets of high-energy TiO_2 nanocrystals exhibit different band configurations, and these co-exposed {101} and {001} facets of nanocrystals establish unique surface heterojunctions within single particles of TiO_2 that are advantageous for the rapid transfer of photo-induced electrons. In addition, building 3D/2D heterojunctions between two contact semiconductors with profound and broad facet-dependent contact areas will provide more effective gap and improved the efficiency as claimed by Cao et al. [20]. Through efficient synthesis of TiO_2/g-C3N4 heterojunction composites with a simple calcination route it resulted the photo-generated holes appear to stay in the TiO_2 valence band, while the electrons initially transfer from the conduction band of TiO_2 to the valence band of g-C3N4, which further excited the g-C3N4 VB [190].

Dye sensitization and reactive facet exposure have recently become a successful way to extend the spectrum of light reaction and prolong the lifespan of

photogenerated electrons and holes. Owing to its greatest π-conjugated framework, good thermal stability, and better absorption on visible irradiation, metalloporphyrin is known as one of outstanding photosensitizer. Most of the studies by several researchers involved metalloporphyrin sensitized metal composites [85, 116, 154, 183, 104, 197, 196, 46], has been shown to effectively increase the photocatalytic activity of certain semiconductor materials. Furthermore, metalloporphyrin processes suitable energy levels as one form of organic semiconductor and can comprise effective Z-scheme heterojunction hybrid photocatalysts with n-type TiO_2. This hybrid system will prevent the possibility of recombination of photogenerated charge carriers and boost photocatalytic activity through heterojunction interfaces as claimed by Low et al. [104].

Another study from Jeyalakshmi et al. [68], the team reported that sensitization of cobalt(II) tetraphenylporphyrin controls the electronic configuration in La changed perovskite of $NaTaO_3$, adjusting the bandgap to be narrow bandgap. No major change in the crystal structure of the pristine $NaTaO_3$ nanocubes were observed, but an absorption shift to 330 nm was observed. In addition, sensitization increased the ability to minimize CO_2 and decreased the recombination rate of the charge carrier. After longer irradiation, the material has been shown to be chemically stable. In other works, Zhong et al. [202] reported the effect of exposed catalyst crystal facets on water splitting using CdSe quantum dot (QD) sensitized $BaTiO_3$ nanocubes. They reported that CdSe QDs located on anisotropic planes of (230) and (001) of 30-face cubic of barium titanate exhibited higher efficiency compared to isotropic (001) facets of 6-face cubic of similar perovskite.

13.4.5 Others

Another alternative and practical modification, by involving carbon-based materials due to their appropriate function, large surface areas, good conductivity and chemical stability, as described by Sun et al. [155], Wang et al. [172, 174, 168], Tan et al. [160]. Thus, the electron transfer of p–n heterojunctions is predicted to be strongly promoted to achieve enhanced photocatalytic behaviour when coated with a carbon film. Besides, the conductive carbon layer will also prevent p–n heterojunction nanostructure accumulation, which is helpful for the increased the stability of p–n heterojunctions.

Zhou et al. [203] reported the production of $ATiO_3$ hierarchical structure in 3D utilizing the natural green leaves that aimed to decrease the emission of carbon dioxide in the presence of A: 1⁄4 Sr, Ca and Pb. The porous network provided by leave vein has a wide surface area that enhances gas diffusion, thus improving overall efficiency. Furthermore, with a similar 3D structure, worked with numerous cocatalysts, such as Pt, Cu, NiOx, Au, Ag and RuO_2. The highest evolution of CO and CH_4 among all gold (Au) was observed, followed by Cu and Ag under visible light illumination.

Shi and co-workers [142] have been investigating the impact of the manufacturing approach on the catalytic efficiency of $NaNbO_3$ through a solid-state reaction and hydrothermal. Different morphologies were observed from those reactions. Smooth and straight nanowires produced from hydrothermal reaction while bulk particles in homogenous sizes were formed by solid-state reaction. The two methods provided perovskite with a similar bandgap of 3.4 eV and the activity was examined under UV illumination by the generation of CH4. The homogeneous nanowires with increased crystallinity and greater surface area showed better CH4 behaviour relative to pristine $NaNbO_3$ [142]. Further combination of $NaNbO_3$ nanowires with g-C3N4 steered to greater performance compared to pristine $NaNbO_3$ or g-C3N4 for reduction of carbon dioxide. The overlap of $NaNbO_3$ and C3N4 coordinated band structures increased the efficiency of photocatalytics [142].

By using rGO carbon derivative as an electron separator and transporter to improve H_2 photocatalytic performance in water splitting, Humera et al. [60] further enhanced the production of $LaFeO_3$. The analysis shows that the integration of rGO was able to improve the efficiency of the studied material. In addition, several researchers team like Moniruddin et al. [117] and Dong et al. [31] stated the calcination temperature and the concentration of precursors play a crucial role in improving the photocatalytic perovskite performance. The study of Moniruddin et al. [117] found the size of $SrTiO_3$ is greatly increased with heating temperatures up to 800 °C. The H_2 production rate increases as the temperature rises. It can be seen that with increasing precursor concentration in EtOH at 800 °C, the H_2 production rate reduces simultaneously as the size of $SrTiO_3$ decreases.

The effect on the size and structure of $CaTiO_3$ by changing the temperature, molar ratio of water to ethanol and reaction time was successfully studied by Dong et al. [31]. The shape varies from inhomogeneous structure to microspheres with longer reaction time and temperature elevation. The morphology of microspheres demonstrated greater photocatalytic activity as opposed to randomly aggregated nanosheets [31]. The growth in photocatalytic activity is largely due to the greater redox potential of $CaTiO_3$. The synergistic impact of morphology and visible facets in a photocatalytic system is therefore crucial to determine the efficiencies of photocatalyst [202].

13.5 Application of Perovskite Photocatalyst

13.5.1 Water Purification

Water purification is the process of discarding contaminants from water such as algae, bacteria, fungi, viruses as well as parasites as in a biological group, meanwhile in the chemical group consists of organic pollutants, inorganic pollutants, toxic metals and suspended solids. Conventional purification processes use filtration

and adsorption to remove the impurities from water sources. However, there are several problems encountered, such as producing secondary waste, needing extra treatment to unclog the filter and the pollutant not completely degraded. Therefore, photocatalysis provides new insight into the water purification process. Due to the ability of photocatalyst in degrading pollutants, it overcomes all the drawbacks of conventional processes.

Figure 13.2 shows the basic mechanism of water purification by the photocatalysis process. The general photocatalysis process by perovskite photocatalyst describe as following (i) the photon from light source hit the perovskite photocatalyst surface and produce electrons and holes; the light energy must overcome the band gap in order to produce electrons and holes (ii) electron travel to the conductive band (CB), simultaneously hole travelled to valence band (VB) (iii) holes react with water molecules to produce hydroxyl ions and hydrogen ions. Further reaction of hydroxyl ions with holes produce hydroxyl radicals which are an active species to degrade the pollutants (iv) simultaneously, electrons react with electrophilic oxygen to form superoxide radical anions also one of active species. When superoxide reacts with hydrogen ions, create hydroperoxyl radicals. Two hydroperoxyl radicals react, forming the hydrogen peroxide. Hydrogen peroxide acts as fuel in producing an abundance of hydroxyl ions and hydroxyl radicals. Therefore, most of the pollutants can be degraded when they react with these active species and usually produce oxygen, carbon dioxide, water among the end products.

When light source hit the perovskite photocatalyst surface,

Perovskite photocatalyst + *hv* $\rightarrow$ $h^+ + e^-$ (*perovskite photocatalyst*)

At CB,

$$h^+ + H_2O \rightarrow OH^- + H^+$$

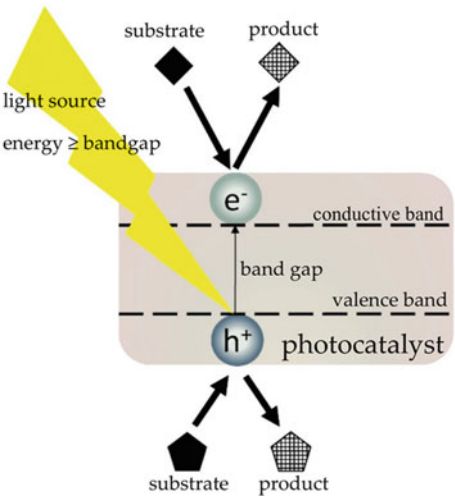

Fig. 13.2 Basic mechanism of perovskite photocatalysis [112]

$$h^+ + OH^- \rightarrow {}^{\bullet}OH$$

Simultaneously, at VB,

$$e^- + O_2 \rightarrow O_2^{\bullet -}$$

$$O_2^{\bullet -} + H^+ \rightarrow HO_2^{\bullet}$$

$$HO_2^{\bullet} + HO_2^{\bullet} \rightarrow H_2O_2 + O_2$$

$$H_2O_2 + O_2^{\bullet -} \rightarrow {}^{\bullet}OH + OH^- + O_2$$

$$H_2O_2 + e^- \rightarrow {}^{\bullet}OH + OH^-$$

Therefore, after generate the active species,

The pollutants + specific active species → degradation products

Absalan et al. [1] synthesis to degrade bromophenol blue wastewater. The band gap was found at 3.80 eV required visible light of 410 W halogen lamp. In 120 min, 0.05 mol perovskite photocatalyst dosage successfully degraded 82% of 10.5^{-14} mol/L bromophenol blue solution. The reaction was repeated for 3 cycles to prove the stability of that perovskite photocatalyst. Due to high crystallinity and highly photoinduced, $CoTiO_3$ creates electrons at CB and holes at VB after obtaining the required light source. At the surface, the same mechanism as previously stated in general perovskite photocatalysis was observed in degradation of bromophenol blue solution. Meanwhile, Fig. 13.3 shows the mechanism of $BaBiO_3$ perovskite photocatalyst in degradation of Rhodamine B wastewater. 0.5 g/L of perovskite photocatalyst is able to tackle 5 mg/L of Rhodamine B solution by both discoloration (83%) and mineralization (80%) within 240 min and shows high stability for 4 cycles of reaction under visible light (450 W Xenon lamp). Active species generated by excitation of $BaBiO_3$ (2.02 eV band gap) such as holes, hydroxyl and superoxide radicals, break the aromatic rings to form smaller molecular weight and intermediates, which further reaction produce the end products such as CO_2, NH_4^+ and water. It proves that perovskite photocatalyst can enhance the charge mobility in the crystalline network due to high crystallinity, the low particle size promotes short diffusion length of the charge carrier to reach the photocatalyst surface and reduce the electron-hole recombination [59].

Doped-perovskite photocatalysis for water purification shows a different mechanism. Usually, the doping acts as an electron trapper to avoid electron-hole recombination. Therefore, the electron acceptor such as diffuse oxygen can easily trap electrons to produce superoxide radicals and other active species to degrade pollutants. It is observed by Wang et al. [176, 171], 91.4% of 48 mg/L rhodamine B wastewater degraded within 120 min under visible light (300 W Xenon lamp) by $Bi/BiOCl/ZnSn(OH)_6$ doped-perovskite photocatalyst. Figure 13.4 two-part energy level for Bi/BiOCl and $ZnSn(OH)_6$; Firstly, light energy hit BiOCl to produce electrons at CB and holes at VB. Due to Fermi level of Bi is lower than CB of

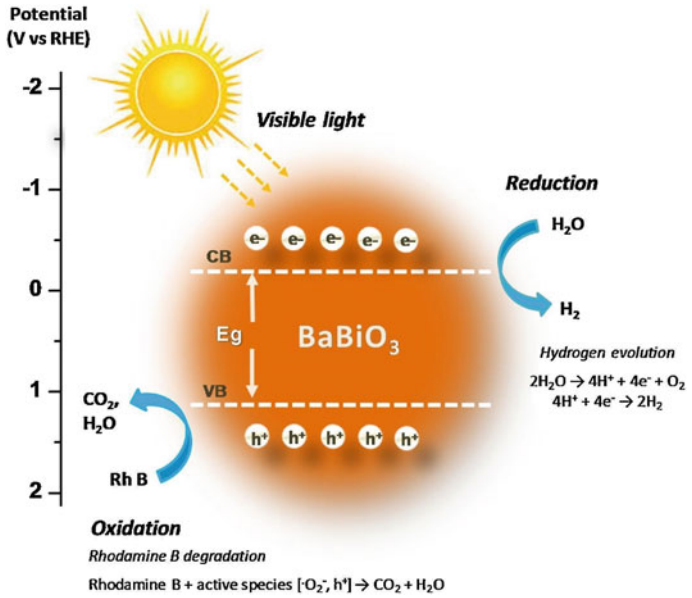

Fig. 13.3 Mechanism of $BaBiO_3$ perovskite photocatalyst in Rhodamine B wastewater degradation and hydrogen production [59]

BiOCl, the electron trap at Bi-metal instead. Then, the electrons transfer to ZnSn $(OH)_6$ and react with diffuse oxygen to produce superoxide. The superoxide further reacts and produce hydroxyl radicals to degrade Rhodamine B molecules partly into water and CO_2. Interestingly, at dopant, due to the accumulated electrons, the same mechanism also applied to produce hydroxyl radicals and able to degrade Rhodamine B. Next, the holes created by perovskite photocatalyst act as powerful active species to directly degrade Rhodamine B molecules. Aligned with Safari et al. [135], the methylene blue molecules purified by photogenerated holes and superoxide anion radicals produced by Gd-doped $NiTiO_3$. The doping of gadolinium (Gd) ion helps in improving the porosity of $NiTiO_3$ perovskite photocatalyst by decreasing the perovskite size, improving the specific surface area and reducing the recombination of electron-hole. Thus, it enhanced the production of holes and superoxide anion radicals. Therefore, the degradation of methylene blue achieved 88.64% within 120 min.

$$Gd^{3+} + e^- \rightarrow Gd^{2+} \text{(electron trapping step)}$$

$$Gd^{2+} + O_{2(ads)} \rightarrow Gd^{3+} + O^{\bullet -}_{2(ads)} \text{(electron transferring step)}$$

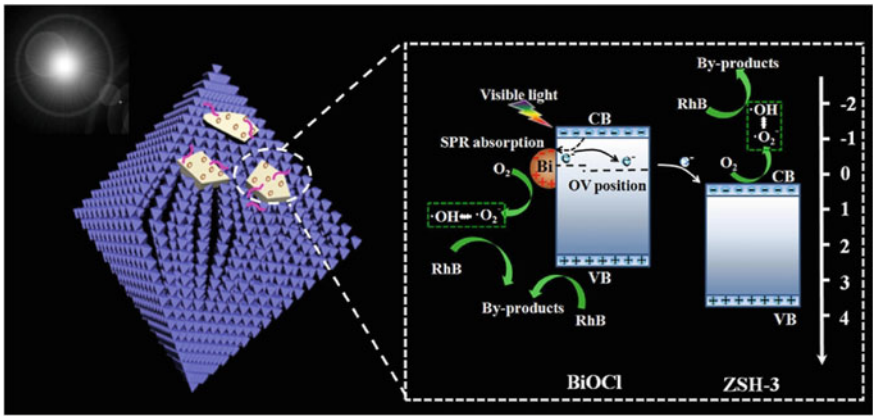

Fig. 13.4 Doped-perovskite photocatalyst [176, 171]

$$O^{\bullet-}_{2(ads)} + H^{+}_{(ads)} \rightarrow HO^{\bullet}_{2(ads)}$$

$$HO^{\bullet}_{2(ads)} + H^{+}_{(ads)} + e^{-} \rightarrow H_2O_2$$

$$H_2O_{2(ads)} + e^{-} \rightarrow {}^{\bullet}OH_{(ads)} + OH^{-}_{(ads)}$$

13.5.2 Bacteria Disinfection and Air Purification

Bacteria is a unicellular microorganism from prokaryote group. It can be divided into two types: gram-positive and gram-negative. Gram-positive bacteria have a thick cell wall made of peptidoglycan, meanwhile gram-negative bacteria have a cell wall made from outer membrane and thin peptidoglycan layer. Bacteria disinfection is physical or chemical treatment to reduce bacteria amount until obtaining desired concentration. Bacteria disinfection by photocatalysis can be achieved when the light source hits the perovskite photocatalyst to generate electrons and holes. In the CB, there are two paths to deactivate the bacteria. Powerful active species in deactivating bacteria is superoxide radicals which produce when electrons react with oxygen. In the presence of water molecules, superoxide radicals can react with it to create another active species, hydroxyl radicals to deactivate the bacteria. Meanwhile, at VB, the holes itself have the ability to deactivate the bacteria directly.

At CB,

$$e^- + O_2 \rightarrow O_2^{\bullet -}$$

$$O_2^{\bullet -} + \text{bacteria} \rightarrow \text{deactivated bacteria}$$

$$O_2^{\bullet -} + H_2O \rightarrow {}^{\bullet}OH$$

$${}^{\bullet}OH + \text{bacteria} \rightarrow \text{deactivated bacteria}$$

Simultaneously at VB,

$$h^+ + \text{bacteria} \rightarrow \text{deactivated bacteria}$$

The study by Shi et al. [145] found that $CuBi_2O_4/Bi_2MoO_6$, a perovskite photocatalyst (Bi_2MoO_6) with heterojunction p-type semiconductor ($CuBi_2O_4$), disinfect *Escherichia coli* (*E. coli*) almost completely within 4 h under visible light. Figure 13.5 shows the mechanism of photocatalytic disinfection that produces the active species such as holes, superoxide radicals, and hydroxyl radicals to inactivate *E. coli*. The band gap of perovskite photocatalyst is 2.72 eV can highly absorb 420 nm visible light and create the holes after the electrons excite to CB. At CB of perovskite photocatalyst, the electrons accumulate and follow the same paths as the stated general mechanism to produce superoxide radical and hydroxyl radicals for bacteria deactivation. Concurrently, the holes accumulate at p-type semiconductor attack the cell membrane and cause the inactivation of *E. coli*. The large specific surface area of $CuBi_2O_4/Bi_2MoO_6$ provides a more reactive site and reaction interface between photocatalyst and the bacteria. Hence, slow recombination rate,

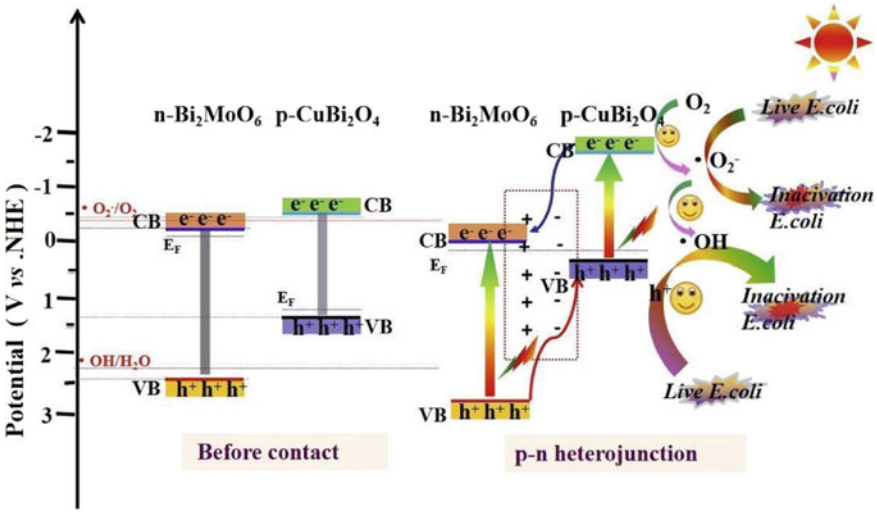

Fig. 13.5 Photocatalytic disinfection mechanism of *E. coli* by $CuBi_2O_4/Bi_2MoO_6$ [145]

high efficiency for separation, high utilization rate of light and large specific surface area are the valuable characteristics for photocatalyst during photo-disinfection. Meanwhile, Li et al. [93], study the application of perovskite photocatalyst for both gram-positive and gram-negative under the same factors. Under 400 nm visible light (300 W Xenon lamp) irradiation, *E. coli* gram-negative and *Staphylococcus aureus* (*S. aureus*) gram-positive were successfully degraded by Pb–$BiFeO_3$/rGO. The complete inactivation of *E. coli* within 30 min, meanwhile *S. aureus* achieved 99.7% degradation within 90 min. Gram-positive is more highly resistant due to their cell wall structure, made up of 3D spatial network structure composed of many layers of teichoic acids and peptidoglycan compare to gram-negative bacteria consists of single layer scattered structure only.

Air purification is a process to kill airborne pathogens that can cause airborne disease to humans or animals such as allergies, influenza, flu and measles. The treatment reaction must be able cut-off the spread routes of pathogens either via aerosol or contaminated fluid. The perovskite photocatalyst, $La_{0.9}MnO_3$ demonstrates high oxidative ability towards influenza A virus. The illustration in Fig. 13.6 shows hemagglutinin and neuraminidase, the amino acid residue of envelope proteins on influenza virus oxidized by $La_{0.9}MnO_3$. The oxidative species might penetrate the virus and damage the genetic materials. In 15 min, almost 76% of the virus has been disinfected. Therefore, prefer features of perovskite photocatalyst as air purifier utilize visible light despite of UV light due to its carcinogenic potential to humans and animals, able to self-disinfecting the airborne pathogens without requiring external energy sources and working continuously, less harsh and also high stability.

13.5.3 Photocatalytic Hydrogen and Oxygen Production

Hydrogen energy is the latest renewable energy discovered by scientists in this century. In the meantime, it was developed for the purpose of hydrogen vehicles that use internal combustion engines and fuel cells that are still under progress and expected extensive study. The benefits of this approach are low greenhouse gas emissions and can obtain by various fuel sources. For energy storage, gives economic benefits due to efficient remote power systems and also reduction in production and operational costs compared to fossil fuel energy.

Photocatalytic hydrogen evolution requires electrons as major active species. Water splitting is a reversible process in hydrogen and oxygen production, so photocatalyst is introduced in the reaction in order to produce an abundance of hydrogen gas that can be collected.

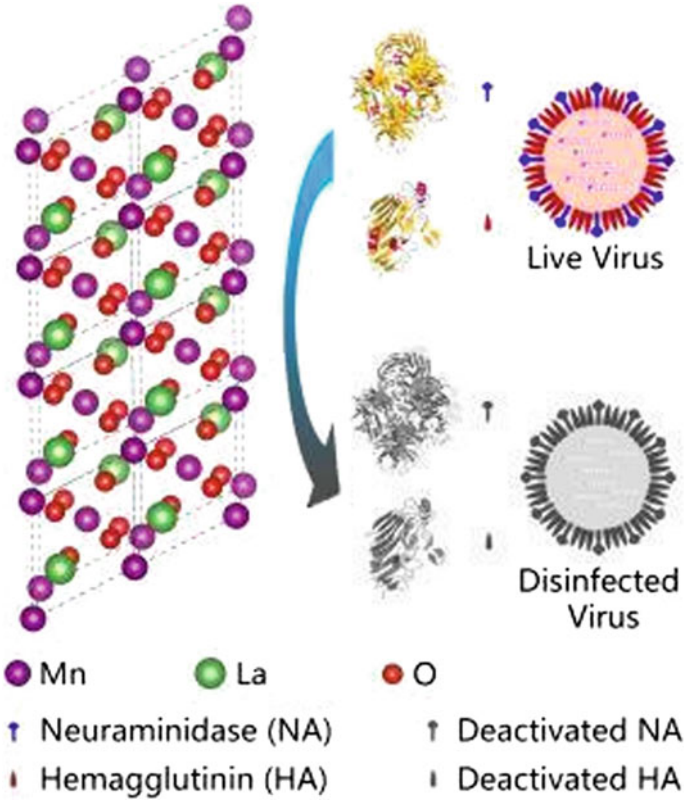

Fig. 13.6 Deactivation of amino acids residue of envelope proteins influenza A virus by $La_{0.9}MnO_3$ perovskite photocatalyst [179]

Water splitting by exert energy

$$2H_2O + \text{energy} \rightleftarrows 2H_2 + O_2$$

In presence of photocatalyst, at CB, water molecules reduce to form hydrogen gas

$$2H_2O + 2e^- \rightarrow H_2 + 2OH^-$$

And water molecules oxidize to form oxygen gas

$$2H_2O + 4h^+ \rightarrow O_2 + 4H^+ + 4e^-$$

Existing research recognizes the critical role played by perovskite photocatalyst in hydrogen and oxygen production. $BaBiO_3$ produces 61 μmol g^{-1} h^{-1} hydrogen gas in 3 h under irradiated 450 W Xenon visible lamp. The water molecule is

reduced to produce hydrogen gas, meanwhile it is oxidized to form oxygen gas as shown in Fig. 13.3.

Water molecule reduction to form hydrogen gas

$$2H_2O \rightarrow 4H^+ + 4e^- + O_2$$

$$4H^+ + 4e^- \rightarrow 2H_2$$

This perovskite photocatalyst synthesis with slow and good crystal growth with a less formation of defects. The defects can act as a recombination center. Thus, the high crystallinity promotes better electrons and holes mobility in the crystal network to reach the surface. Next, the particle is small in size to decrease the diffusion length of photogenerated charges transfer to the surface, short distance directly related to low resistance. It also implies low probability for electron-hole pair recombination. Furthermore, small particles contribute to high surface area and increase the adsorption capacity between perovskite photocatalyst and water molecules. Hence, the stable photocatalytic hydrogen evolution must be attributed to high crystallinity, low particle size, low recombination of electron-hole and low resistance to improve the hydrogen production.

13.5.4 Photocatalytic Reduction of CO_2

Almost 77% of carbon dioxide emission mainly contributed by transportation, electricity and industry was reported by the United States Environmental Protection Agency (EPA) due to large consumption of limited fossil fuels. Therefore, the endeavour to convert CO_2 into chemical fuels such as carbon monoxide, methane and methanol to solve the global energy and environmental issues. Photocatalysis has been recognized as one of promising strategies to tackle this problem. As artificial photosynthesis, photocatalysts utilize solar energy to combine with CO_2 and H_2O to produce the chemical fuels and carbon monoxide as shown in Fig. 13.7.

As shown in Fig. 13.8, there are two paths for CO_2 reduction either as CO or CH_4 can be achieved simultaneously during photocatalytic reactions. The influence of H^+ ion amounts towards CO_2 molecules play an important role for the end product yields. When the light reaches $SrTiO_3$ perovskite photocatalyst, the electrons excite to CB leaving the holes on VB. The active species on VB react with H_2O to produce H^+. Meanwhile, the electrons at CB transfer to the dopant, Pt and react with H^+ to produce CO and CH_4.

$$CO_2 + 2H^+ + 2e^- \rightarrow CO + H_2O \left(E^\theta = -0.53\ V\right)$$

$$CO_2 + 8H^+ + 8e^- \rightarrow CH_4 + 2H_2O \left(E^\theta = -0.24\ V\right)$$

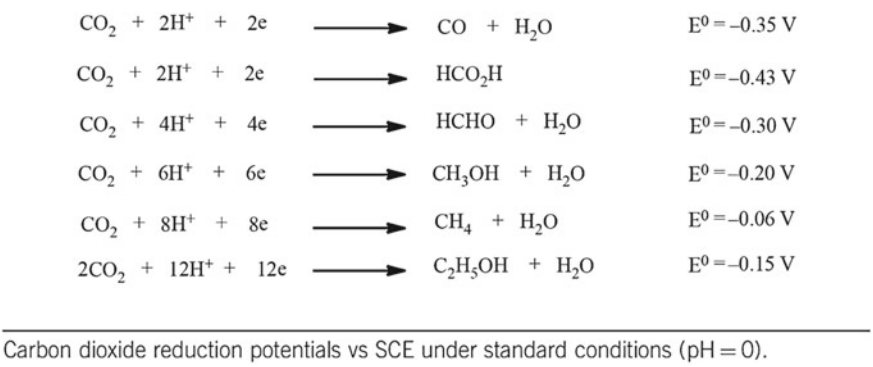

Fig. 13.7 List of carbon dioxide reduction reactions produce different chemical fuel products [185]

Meanwhile, the morphology of perovskite photocatalysts influences light harvesting. The 3D ordered macroporous (3DOM) morphology of $SrTiO_3$ perovskite photocatalyst improves the light absorption by slowing the light source from reaching Pt/$SrTiO_3$ and separating the charge carriers. Next, the alkali earth metal, Sr in the $SrTiO_3$ helps the adsorption and initiate activity for CO_2 reactant due to high alkalinity of Sr. The Pt dopant helps to separate the photogenerated charges by transferring the electrons and react directly with H^+ ions. Therefore, perovskite photocatalyst shows potential in CO_2 reduction by undergoing artificial photosynthesis.

13.5.5 Application of Visible-Light-Driven Perovskite as Photovoltaic Solar Cell (PSCs)

Current global power demand is increasing significantly every year aligned with the improvement of the technologies and industries need. Nowadays it was reported that the energy usage is 16TW globally and expected to increase up to 30TW in 2050 [133]. Therefore, a lot of research has been done since then with only one purpose to find an alternative source that can add-on to the current or conventional source of energy such as petroleum-based fuel. Among the various sources of energy, solar energy was found to be the most significant and promising since it is easily and readily available. This is possible by converting the solar energy to electricity. Therefore, using photovoltaic solar cells for power generation seems to be a promising way as they convert the sunlight directly into electricity.

Nowadays, the market was dominated by the crystalline silicon solar cells. However, the production of the solar cells is costly due to the expensive raw materials. Because of that, most of the researchers come up with new ideas of utilizing PV technology that has low efficiency and cost manufacturing. Despite all

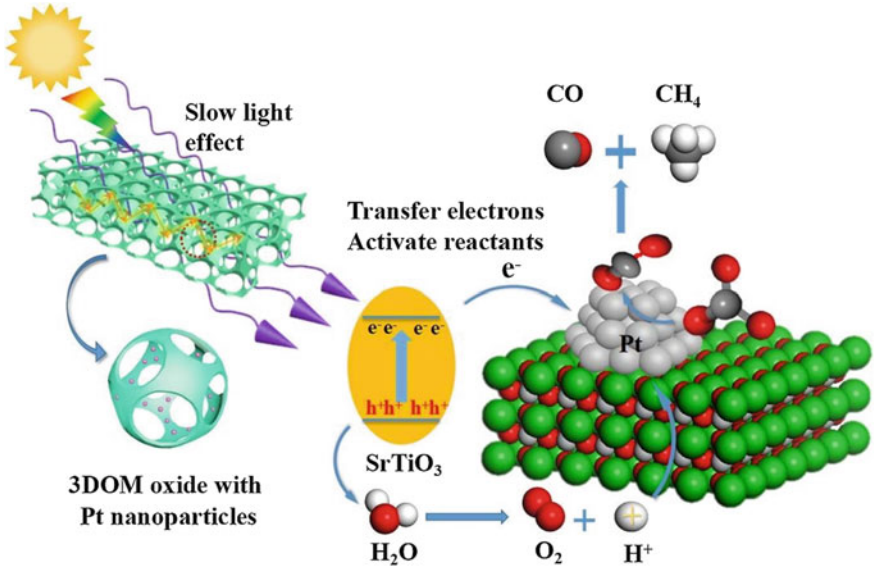

Fig. 13.8 The mechanism of Pt doped $SrTiO_3$ perovskite photocatalyst in carbon dioxide reduction into carbon monoxide and methane [180]

the facts, poor device stability and short lifetime are creating interferences in the path of commercialization of PSCs, the perovskite materials are gaining huge attention among the researchers because of their excellent PV performance, cheap raw material, and requires of easy processing parameters [205]. Furthermore, it also does not entail any complicated processing conditions, since it can be created by using simple low-cost methods such as screen printing, dual-source evaporation, spin and dip coatings techniques which can be developed on flexible substrate.

Si et al. [147] have studied the fundamentals on the absorption of PSCs. It was found that the perovskite layer tends to absorb UV and visible light bands, meanwhile, the electrode layer favours to absorb IR bands. Interestingly, plasmonic was used to create hot spots in active layer via light-flow-circulating and nonlinear absorption mechanisms so that, the light can be localized through perovskite material. Si et al. [147] also reported that the absorption of IR-band has been extended to 58.2% when the plasmonic was used in the materials.

Figure 13.9a, b shows the mesoscopic architecture and the planar heterojunction structure of PSCs, respectively. Recently, the mesoporous materials have been studied and applied as PSCs due to their high porosity and large specific surface area up to 1000 m^2/g [205]. It potentially increases the light response of photo-sensitize material and improves the effectiveness of the instrument.

Basically, a solar cell consists of metal electrode layer, a hole transport layer as Hole Transporting Material (HTM), a perovskite layer, a porous oxide layer, a dense electron transport layer as Electron Transporting Material (ETM), and

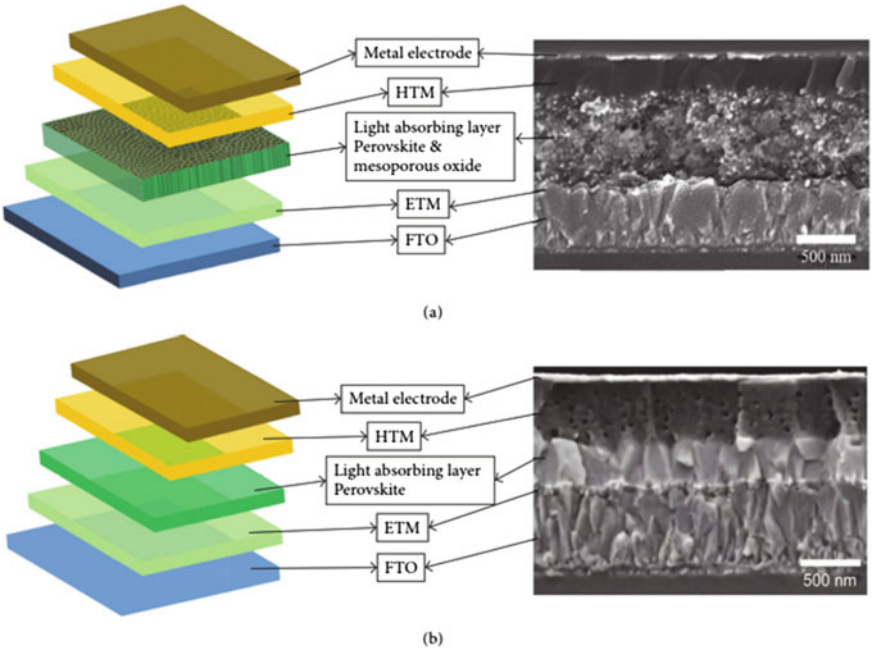

Fig. 13.9 Schematic diagram and SEM section image of **a** mesoscopic architecture PSCs and **b** planar heterojunction structure PSCs (adapted from [205]

Flourine-doped Tin Oxide (FTO) electrode. This structure arrangement not just effective to decrease the recombination rate of electrons and holes, but also provides the necessary diffusion length for the accumulation of electrons and holes effectively [34]. The TiO_2 layer in the middle layer plays a significant function such as conducting the electrons, blocking the holes and inhibits the electron-hole pairs recombination in the FTO conductive substrate. Thus, it contributes to improve the photoelectric conversion efficiency of the studied materials. Furthermore, other than TiO_2, materials like ZnO, Al_2O_3, and ZrO_2 are typically used. Meanwhile, the function of hole transport layer is to accept the generated holes and transfer them to the surface of the metal electrodes. Commonly, the hole transport material and counter electrode materials are Spiro-OMeTAD (2,2',7,7'-Tetrakis [N,N-di (4-methoxyphenyl)amino]-9,9'-spirobifluorene) and noble metals, such as Au, Ag, and Pt, respectively.

Based on Fig. 13.9b, the distinction from the mesoscopic structure is that the planar structure has no porosity of materials between the two layers of the electron transport and the hole transport, as a result, the electron-hole pairs can be parted effectively. Additionally, it contributes enlightenment the mechanisms of light absorption and electron-hole separation, thus, enhance the versatility of device optimization for the development of highly effective and advanced coated perovskite solar cells.

Latest research by Ren et al. [130] they studied power conversion efficiency and efficient light capture and prepared the ultraviolet-ozone assisted strategy on the TiO_2 interface for perovskite solar cells. Interestingly, the modified perovskite PSCs with ultraviolet ozone TiO_2 efficiently suppress the decomposition of perovskite films under light illumination. They found that this device has better performance and remarkable stability as compared to the pristine perovskite solar cells.

13.5.6 Application of Visible-Light-Driven Perovskite as Photocatalytic Nitrogen Fixation

Ammonia (NH_3) is an essential and important substance in the present-day industry as the major component of production of many types of chemicals such as fertilizers and bleaching agents for the cleaning process. Conventionally it has been produced in big scale industries via Haber-Bosch reaction, which requires very high temperature ranging from 400 to 500 °C and pressure ranging from 15 to 25 Mpa [195]. Recently, numbers of research papers reported on the new and advanced techniques which are simpler and environmentally friendly known as nitrogen fixation. Previously, biological nitrogen fixation was introduced and applied in many applications. During this process, the nitrogen gas from the environment will be activated by the organism to produce NH_3 at ambient temperature and pressure, for example of the organism is nitrogenase enzymes which catalyze the reduction of N_2 to NH_3 [19]. Recently, artificial solar-powered nitrogen fixation was introduced, where the concept is by using the energy from light source such photons to excite electron which will be used to create radicals. This can be divided into two major steps; step (i) semiconductor is excited under light irradiation producing photogenerated electrons excited to the CB leaving holes in the VB. Step (ii) the photogenerated holes oxidize water to O_2 while the photogenerated electrons reduce N_2 to NH_3. Figure 13.10 shows the mechanism for the production of NH_3 by using the photocatalytic N_2 fixation technique.

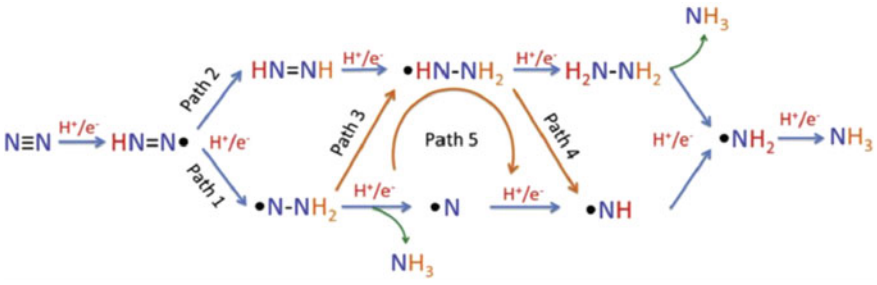

Fig. 13.10 Propose mechanism for the photocatalytic N_2 reduction [195]

As reported by Li et al. [91], the bismuth molybdate nanosheet with oxygen vacancies can be prepared via NaOH etching treatment at room temperature. The function of oxygen vacancies is to boost the photocatalytic nitrogen fixation to produce ammonia under the visible light source at room temperature and ambient pressure. They found that the oxygen vacancies had improved the photogenerated charge carrier separation and improve the capability of the materials for the N_2 adsorption and activation. As a result, production of ammonia was increased up to 800 μmol g^{-1} h^{-1}. Furthermore, these materials also show a good tolerance to the oxygen in the N_2 source for the replacement of pure N_2 with air under simulated solar conditions. The pictorial illustration of relaxed slab model of BMO sample and the Vo–BMO–OH sample surfaces and the schematic representation of photocatalytic N_2 fixation process under visible light illumination is shown in Fig. 13.11.

Wang et al. [176, 171], reported the importance of oxygen vacancies with abundant localized electrons, where it can assist or improve the ability of the material to capture and activate N_2. They proved that the bismuth oxybromide-based semiconductor that they have prepared produced higher NH_3 generation with rate up to 1.38 mmol h^{-1} g^{-1} under visible-light-induced OVs. It also resulted in the stable photoreduction of atmospheric N_2 into NH_3 in pure water, which serves as both solvent and proton source. Figure 13.12 shows that the photocatalytic N_2 fixation of the Bi_5O_7Br–NT can be divided into 4 major steps; (i) under visible light irradiation, part of the O will escape in the form of O_2 from the surface of Bi_5O_7Br–NT creating sufficient surface OVs, (ii) the N_2 is chemisorbed and activated on the OV sites, (iii) the excited electrons s injected into the activated N_2 and reduce it to NH_3 and the last step (iv) the photoinduced OVs would be refilled by seizing O atoms from water, leading to a good recovery to the original stable OV-free composition.

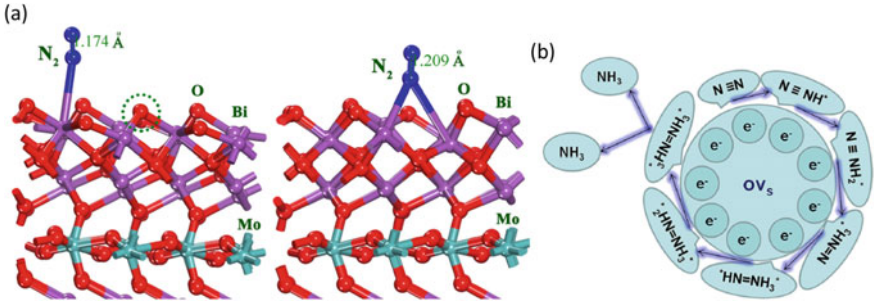

Fig. 13.11 Illustration of **a** the pictorial views of a relaxed slab model for the BMO sample and the Vo–BMO–OH sample surfaces, and **b** the schematic illustration of the photocatalytic N_2 fixation process on the Vo–BMO–OH sample under visible light illumination [91]

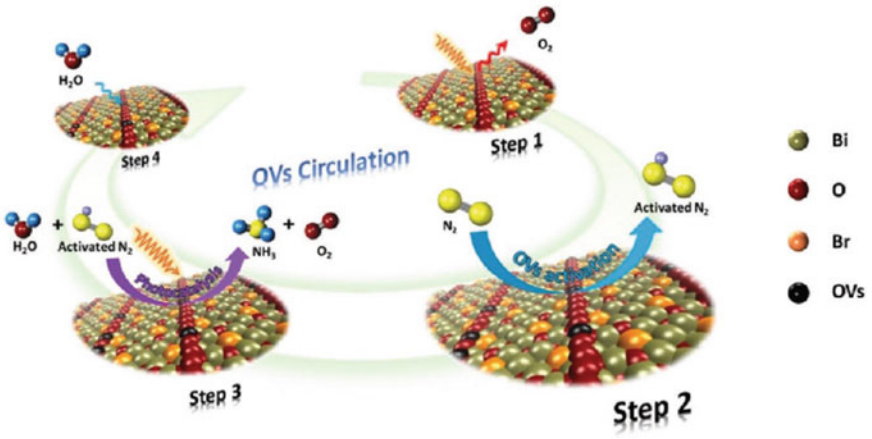

Fig. 13.12 Schematic illustration of the photocatalytic N_2 fixation model in which water serves as both the solvent and photon source as well as the reversible creation of light-induced OVs [176, 171]

13.5.7 Application of Visible-Light-Driven Perovskite Photocatalyst for Anti-fogging Glass

Fog or fogging phenomenon is the formation of small water droplets from the water condensation on the surface of glasses, goggles, camera lenses and binoculars. This is possible due to high surface tension resulting in a single droplet of water. Here, anti-fog or antifogging is very useful to avoid or to reduce the fogging phenomena, it can be done by reducing the surface tension and altering the degree of wetting by introduction of antifogging film, resulting in the super hydrophilic, non-scattering film or water instead of droplets.

Takata et al. [158], reported that they prepared the antifogging glass by coating the glass with the TiO_2 layer. It was observed that the TiO_2 has super hydrophilic properties which is very likely attracted to water other than common ability such as anti-bacterial, anti-pollution and deodorant materials. They mentioned that when the surface of TiO_2 is irradiated with UV-light could decrease the contact angle (CA) and reaches almost zero with time as illustrated in Fig. 13.13 where the incident light will not be diffracted. This finding also aligned with the statement reported by Duan et al. [32] stated that the super hydrophilic TiO_2 film reduces the CA 150° (hydrophobic TiO_2) to less than 5° (hydrophilic TiO_2). When the TiO_2 coated glass expose to the condensed water, the droplets will create or form very thin water film and become transparent, automatically, due to the self-cleaning effect it will repel oil layer and when exposed to the light source it activated and catalyzed the degradation of any possible bacteria and fungi, etc. Because of that ability, it was known that the TiO_2 has vast application as antifogging and also the antibacterial or self-cleaning assisted material.

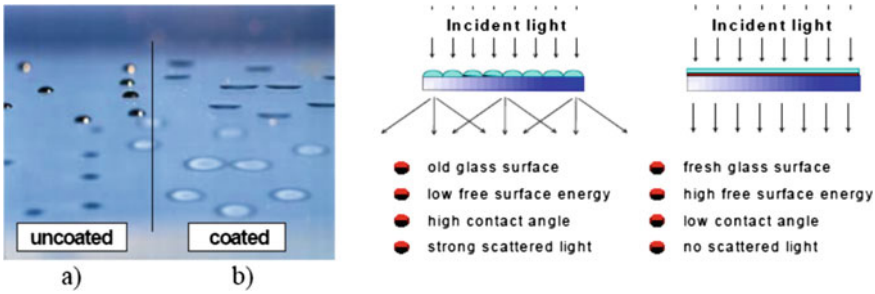

Fig. 13.13 Illustration of water drops on a glass surface **a** uncoated side: hydrophobic (CA = 65°) and **b** coated side: hydrophilic (CA < 10°)

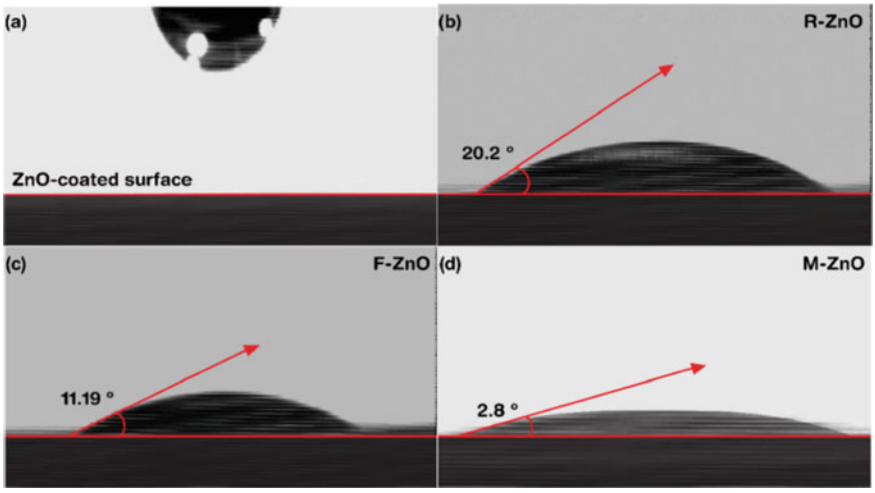

Fig. 13.14 Contact angle measurement (CA) of **a** water drop before contact to the ZnO-coated surface; **b** nanorods ZnO, **c** microflowers ZnO, and **d** porous microspheres ZnO [119]

Nundy et al. [119] studied the performance of the super hydrophilic ZnO microstructure coating for photovoltaic and glazing applications. They reported on the wettability and photovoltaic behaviour can be affected by the different structures of ZnO by affecting the CA of each structure as shown in Fig. 13.14. From this Figure, we can see that the hydrophilic surfaces for nanorods ZnO with higher CA and super hydrophilicity of microflower and microsphere ZnO with lesser CA, respectively. This is due to the changes of crystallinity and microstructural during the synthesis of ZnO. Thus, microstructure ZnO is good for the many antifogging and photovoltaic applications.

According to Takagi et al. [157], there are numbers of application of TiO_2 that has been studied as the sterilizer, cleaner, decomposer, and antifogging agent. This

is because of the TiO_2 that has high oxidizing power when it is irradiated by solar light. They also studied the sputter deposition technique to apply the TiO_2 film on the surface of the glass or any targeted clean surface. Based on our previous studies, a lot of research papers were discussed on the potential of photocatalyst as an antifogging agent by increasing the wettability and reducing the contact angle of the surfaces especially TiO_2 and ZnO. However, best in our knowledge, studies on the perovskite structure of photocatalyst as potential antifogging glass is not yet reported or discussed elsewhere. This will become a good opportunity for the researchers to study, evaluate and conduct research on the application of perovskite photocatalyst as the antifogging agent.

13.6 Conclusion

This chapter revealed the theory of perovskite-based photocatalyst for various environmental remediation applications specifically under visible light and solar irradiation. Moreover, the different type of perovskite materials together with its advantages is thoroughly discussed. Its unique characteristic enables it to incorporate with other metal and non-metal nanomaterials and such modification strategies leads to an improve ability of perovskite-based photocatalyst especially in harvesting of visible or solar light and prolong the life span of the charge carriers has been further explained. The promising outcome of the fabrication perovskite materials and its development pathway for various applications for energy conversion and other environmental applications. Hence, the perovskite-based photocatalysts are a versatile material in terms of its recurrent development that enable performance enhancement and its practicality towards environment protection in the time ahead.

References

1. Absalan Y, Alabada R, Ryabov M, Tolstoy V, Butusov L, Nikolskiy V, Kopylov V, Gholizadeh M, Kovalchukova O (2020) Removing organic harmful compounds from the polluted water by a novel synthesized cobalt(II) and titanium(IV) containing photocatalyst under visible light. Environ Nanotechnol Monit Manag 14:
2. Adnan MAB, Arifin K, Minggu LJ, Kassim MB (2018) Titanate-based perovskites for photochemical and photoelectrochemical water splitting applications: a review. Int J Hydrogen Energy 43(52):23209–23220
3. Ahmad T, Farooq U, Phul R (2018) Fabrication and photocatalytic applications of perovskite materials with special emphasis on alkali-metal-based niobates and tantalates. Ind Eng Chem Res 57(1):18–41
4. Alammar T, Hamm I, Wark M, Mudring A-V (2015) Low-temperature route to metal titanate perovskite nanoparticles for photocatalytic applications. Appl Catal B 178:20–28
5. Aman D, Zaki T, Mikhail S, Selim S (2011) Synthesis of a perovskite $LaNiO_3$ nanocatalyst at a low temperature using single reverse microemulsion. Catal Today 164(1):209–213

6. Anandan S, Ohashi N, Miyauchi M (2010) ZnO-based visible-light photocatalyst: band-gap engineering and multi-electron reduction by co-catalyst. Appl Catal B Environ 100:502–509
7. Andrei V, Reuillard B, Reisner E (2020) Bias-free solar syngas production by integrating a molecular cobalt catalyst with perovskite–$BiVO_4$ tandems. Nat Mater19
8. Anzai A, Fukuo N, Yamamoto A, Yoshida H (2017) Highly selective photocatalytic reduction of carbon dioxide with water over silver-loaded calcium titanate. Catal Commun 100:134–138
9. Arun B, Akshay V, Mutta GR, Venkatesh C, Vasundhara M (2017) Mixed rare earth oxides derived from monazite sand as an inexpensive precursor material for room temperature magnetic refrigeration applications. Mater Res Bull 94:537–543
10. Asahi R, Morikawa T, Ohwaki T, Aoki K, Taga Y (2001) Visible-light photocatalysis in nitrogen-doped titanium oxides. Science 293:269–271
11. Bagvand N, Sharifnia S, Karamian E (2018) A visible-light-active $BiFeO_3$/ZnS nanocomposite for photocatalytic conversion of greenhouse gases. Korean J Chem Eng 35:1735–1740
12. Bahnemann D (2004) Photocatalytic water treatment: solar energy applications. Sol Energy 77:445–459
13. Bai S, Wang L, Li Z, Xiong Y (2017) Facet-engineered surface and interface design of photocatalytic materials. Adv Sci 4:1–26
14. Bai S, Zhang N, Gao C, Xiong Y (2018) Defect engineering in photocatalytic materials. Nano Energy 53:296–336
15. Bajorowicz B, Reszczyńska J, Lisowski W, Klimczuk T, Winiarski M, Słoma M, Zaleska-Medynska A (2015) Perovskite-type $KTaO_3$—reduced graphene oxide hybrid with improved visible light photocatalytic activity. RSC Adv 5(111):91315–91325
16. Balachandran S, Swaminathan M (2012) Facile fabrication of heterostructured $Bi2O_3$-ZnO photocatalyst and its enhanced photocatalytic activity. J Phys Chem C 116:26306–26312
17. Brenner TM, Egger DA, Kronik L, Hodes G, Cahen D (2016) Hybrid organic–inorganic perovskites: low-cost semiconductors with intriguing charge-transport properties. Nat Revi Mater 1:1–16
18. Bresolin B-M, Park Y, Bahnemann DW (2020) Recent progresses on metal halide perovskite-based material as potential photocatalyst. Catalysts 10(6):709
19. Burgess BK, Lowe DJ (1996) Mechanism of molybdenum nitrogenase. Chem Rev 96:2983–3011
20. Cao XR, Tian GH, Chen YJ, Zhou J, Zhou W, Tian CG, Fu HG (2014) Hierarchical composites of TiO_2 nanowire arrays on reduced graphene oxide nanosheets with enhanced photocatalytic hydrogen evolution performance. J Mater Chem A 2:4366–4374
21. Carrasco-Jaim OA, Mora-Hernandez J, Torres-Martínez LM, Moctezuma E (2019) A comparative study on the photocatalytic hydrogen production of $ATiO_3$ (A = Zn, Cd and Pb) perovskites and their photoelectrochemical properties. J Photochem Photobiol, A 371:98–108
22. Chai J, Shen J, Zhang X, Ng YH, Huang J, Guo W, Lin C, Lai Y (2019) Light-driven sustainable hydrogen production utilizing TiO_2 nanostructures: a review. Small Methods 3:1–24
23. Chen K, Schünemann S, Song S, Tüysüz H (2018) Structural effects on optoelectronic properties of halide perovskites. Chem Soc Rev 47:7045–7077
24. Chen S, Huang D, Xu P, Xue W, Lei L, Cheng M, Wang R, Liu X, Deng R (2020) Semiconductor-based photocatalysts for photocatalytic and photoelectrochemical water splitting: will we stop with photocorrosion? J Mater Chem A 8:2286–2322
25. Chen Z, Xing P, Chen P, Chen Q, Wang Y, Yu J, He Y (2018) Synthesis of carbon doped $KTaO_3$ and its enhanced performance in photocatalytic H_2 generation. Catal Commun 109:6–9
26. Chouhan N, Liu R-S, Zhang J (2017) Photochemical water splitting: materials and applications. CRC Press

27. Déak T, Cziġany T (2009) Chemical composition and mechanical properties of basalt and glass fibers: a comparison. Text Res J 79:645–651
28. Demin A, Gorbova E, Brouzgou A, Volkov A, Tsiakaras P (2020) Sensors based on solid oxide electrolytes. Solid Oxide-Based Electrochemical Devices, pp 167–215. Elsevier
29. Ding Z, Guo S, Wu X, Fida H (2018) One-step synthesis of spherical $NaTaO_3$ and graphene spherical $NaTaO_3$ nanoparticles with enhanced photocatalytic activity for NO purification. Funct Mater Lett 11(4):1850070
30. Do JY, Im Y, Kwak BS, Park S-M, Kang M (2016) Preparation of basalt fiber@perovskite $PbTiO_3$ core-shell composites and their effects on CH_4 production from CO_2 photoreduction. Ceram Int 42:5942–5951
31. Dong W, Song B, Meng W, Zhao G, Han G (2015) A simple solvothermal process to synthesize $CaTiO_3$ microspheres and its photocatalytic properties. Appl Surf Sci 349:272–278
32. Duan Z, Zhu Y, Ren P, Jia J, Yang S, Zhao G, Xie Y, Zhang J (2018) Non-UV activated superhydrophilicity of patterned Fe-doped TiO_2 film for anti-fogging and photocatalysis. Appl Surf Sci 452:165–173
33. Dutta SK, Mehetor SK, Pradhan N (2015) Metal semiconductor heterostructures for photocatalytic conversion of light energy. J Phys Chem Lett 6:936–944
34. Edri E, Kirmayer S, Cahen D, Hodes G (2013) High open circuit voltage solar cells based on organic-inorganic lead bromide perovskite. J Phys Chem Lett 4:897–902
35. Fan H-T, Xu X-J, Ma X-K, Zhang T (2011) Preparation of $LaFeO_3$ nanofibers by electrospinning for gas sensors with fast response and recovery. Nanotechnology 22(11):
36. Feldhoff A, Arnold M, Martynczuk J, Gesing TM, Wang H (2008) The sol-gel synthesis of perovskites by an EDTA/citrate complexing method involves nanoscale solid state reactions. Solid State Sci 10(6):689–701
37. Feng Y-N, Wang H-C, Luo Y-D, Shen Y, Lin Y-H (2013) Ferromagnetic and photocatalytic behaviors observed in Ca-doped $BiFeO_3$ nanofibres. Am Inst Phy
38. Frank AJ, Willner I, Goren Z, Degani Y (1987) Improved charge separation and photosensitized H_2 evolution from water with TiO_2 particles on colloidal SiO_2 carriers. J Am Chem Soc 109:3568–3573
39. Fresno F, Jana P, Renones P, Coronado JM, Serrano DP, de la Pena O'Shea VA (2017) CO_2
40. Fu Q, Wang X, Li C, Sui Y, Han Y, Lv Z, Song B, Xu P (2016) Enhanced photocatalytic activity on polarized ferroelectric $KNbO_3$. RSC Adv 6(110):108883–108887
41. Fujiwara T, Sasahara A, Happo N, Kimura K, Hayashi K, Onishi H (2020) Single-crystal model of highly efficient water-splitting photocatalysts: a $KTaO_3$ wafer doped with calcium cations. Chem Mater 32(4):1439–1447
42. Gao C, Wang J, Xu H, Xiong Y (2017) Coordination chemistry in the design of heterogeneous photocatalysts. Chem Soc Rev 46:2799–2823
43. Gao T, Chen Z, Huang Q, Niu F, Huang X, Qin L, Huang Y (2015) A review: preparation of bismuth ferrite nanoparticles and its applications in visible-light induced photocatalyses. Rev Adv Mater Sci 40(2):97–109
44. Garba ZN, Zhou W, Zhang M, Yuan Z (2020) A review on the preparation, characterization and potential application of perovskites as adsorbents for wastewater treatment. Chemosphere 244:125474
45. García-López E, Marcì G, Megna B, Parisi F, Armelao L, Trovarelli A, Boaro M, Palmisano L (2015) $SrTiO_3$-based perovskites: preparation, characterization and photocatalytic activity in gas-solid regime under simulated solar irradiation. J Catal 321:13–22
46. Gomathi Devi L, Nithya PM (2018) Photocatalytic activity of Hemin (Fe(III) porphyrin) anchored $BaTiO_3$ under the illumination of visible light: synergetic effects of photosensitization, photo-Fenton and photocatalysis processes. Inorg Chem Front 5:127–138
47. Grabowska E (2016) Selected perovskite oxides: characterization, preparation and photocatalytic properties—a review. Appl Catal B 186:97–126

48. Guan M, Xiao C, Zhang J, Fan S, An R, Guan M, Xiao C, Zhang J, Fan S, An R et al (2013) Vacancy associates promoting solar-driven photocatalytic activity of ultrathin bismuth oxychloride nanosheets. J Am Chem Soc 135:10411–10417
49. Gundeboina R, Perala V, Muga V (2020) Perovskite material-based photocatalysts. Revolution of Perovskite, pp 251–287. Springer
50. Guo J, Liang J, Yuan X, Jiang L, Zeng G, Yu H, Zhang J (2018) Efficient visible-light driven photocatalyst, silver (meta) vanadate: synthesis, morphology and modification. Chem Eng J 352:782–802
51. Gutiérrez Seijas J, Prado-Gonjal, JS, Ávila Brande D, Terry I, Morán E, Schmidt R (2017) Microwave-assisted synthesis, microstructure, and magnetic properties of rare-earth cobaltites. Inorg Chem 56(1):627–633
52. Han X, Kuang Q, Jin M, Xie Z, Zheng L (2009) Synthesis of titania nanosheets with a high percentage of exposed (001) facets and related photocatalytic properties. J Am Chem Soc 131:3152–3153
53. He Y, Zhu Y, Wu N (2004) Synthesis of nanosized $NaTaO_3$ in low temperature and its photocatalytic performance. J Solid State Chem 177:3868–3872
54. Hong RY, Li JH, Chen LL, Liu DQ, Li HZ, Zheng Y, Ding J (2009) Synthesis, surface modification and photocatalytic property of ZnO nanoparticles. Powder Technol 189:426–432
55. Hou J, Cao S, Wu Y, Liang Fi, Ye Li, Lin Z, Sun L (2016) Perovskite-based nanocubes with simultaneously improved visible-light absorption and charge separation enabling efficient photocatalytic CO_2 reduction. Nano Energy 30:59–68
56. Huan Y, Shen H, Zhu Y, Li M, Li H, Wang Z, Hao Y, Wei T (2019) Enhanced ferro-photocatalytic performance for $ANbO_3$ (A = Na, K) nanoparticles. Math Biosci Eng 16: 4122–4134
57. Huang F, Yan A, Zhao H (2016) Influences of doping on photocatalytic properties of TiO_2 photocatalyst. In: Cao W (ed) Semiconductor photocatalysis—materials, mechanisms and applications. InTech, Rijeka
58. Huang HC, Yang C-L, Wang M-S, Ga Ma X (2019) Chalcogens doped $BaTiO_3$ for visible light photocatalytic hydrogen production from water splitting Spectrochim. Acta, Part A 208:65–72
59. Huerta-Flores AM, Sánchez-Martínez D, Hernández-Romero MDR, Zarazúa-Morín ME, Torres-Martínez LM (2019) Visible-light-driven $BaBiO_3$ perovskite photocatalysts: effect of physicochemical properties on the photoactivity towards water splitting and the removal of rhodamine B from aqueous systems. J Photochem Photobiol, A 368:70–77
60. Humera S, Sara M, Muhammad S, Muhammad Azhar K, Muhammad S, Muhammad Farooq W (2018) Rare earth substituted nanocrystalline $LaFeO_3$ perovskites and their composites with reduced graphene oxide for enhanced photocatalytic and other potential applications Mater. Res Express 5:065062
61. Im Y, Park SM, Kang M (2017) Effect of Ca/Ti ratio on the core-shell structured CaTiO Bull. Korean Chem Soc 38:397–400
62. Ishii T, Anzai A, Yamamoto A, Yoshida H (2020) Calcium zirconate photocatalyst and silver cocatalyst for reduction of carbon dioxide with water. Appl Catal B: Environ 119192
63. Iwasaki T, Shimamura Y, Makino Y, Watano S (2016) Mechanochemically assisted synthesis and visible light photocatalytic properties of lanthanum nickel oxide nanoparticles. Optik 127(20):9081–9087
64. Jaffari ZH, Lam S-M, Sin J-C, Zeng H (2019) Boosting visible light photocatalytic and antibacterial performance by decoration of silver on magnetic spindle-like bismuth ferrite. Mater Sci Semicond Process 101:103–115
65. Jamal M, Bashar M, Hasan AM, Almutairi ZA, Alharbi HF, Alharthi NH, Karim MR, Misran H, Amin N, Sopian KB (2018) Fabrication techniques and morphological analysis of perovskite absorber layer for high-efficiency perovskite solar cell: a review. Renew Sustain Energy Rev 98:469–488

66. Jayapandi S, Lakshmi D, Premkumar S, Packiyaraj P, Anitha K (2018) Augmented photocatalytic and electrochemical activities of Ag tailored $LaCoO_3$ perovskite semiconductor. Mater Lett 218:205–208
67. Jeyalakshmi V, Mahalakshmy R, Ramesh K, Rao PV, Choudary NV, Thirunavukkarasu K, Krishnamurthy KR, Viswanathan B (2018) Metal oxides as photo catalysts: modified sodium tantalate as catalyst for photo reduction of carbon dioxide. Mol Catal 451:105–113
68. Jeyalakshmi V, Tamilmani S, Mahalakshmy R, Bhyrappa P, Krishnamurthy KR, Viswanathan B (2016) Sensitization of La modified $NaTaO_3$ with cobalt tetra phenyl porphyrin for photo catalytic reduction of CO_2 by water with UV–visible light. J Mol Catal A: Chem 420:200–207
69. Jin J, Yu J, Guo D, Cui C, Ho WA (2015) Hierarchical Z-scheme CdS-WO_3 photocatalyst with enhanced CO_2 reduction activity. Small 11:5262–5271
70. Kadi MW, Mohamed RM (2019) Synthesis of $BaCeO_3$ nanoneedles and the effect of V, Ag, Au, Pt doping on the visible light hydrogen evolution in the photocatalytic water splitting reaction. J Sol-Gel Sci Technol 91(1):138–145
71. Kako T, Kikugawa N, Ye J (2008) Photocatalytic activities of $AgSbO_3$ under visible light irradiation. Catal Today 131(1–4):197–202
72. Kako T, Ye J (2010) Synergistic effect of different phase on the photocatalytic activity of visible light sensitive silver antimonates. J Mol Catal A: Chem 320(1–2):79–84
73. Kamat PV (2015) All Solution-Processed Lead Halide Perovskite-$BiVO_4$ tandem assembly for photolytic solar fuels production. J Am Chem, Soc, p 137
74. Kanhere P, Chen Z (2014) A review on visible light active perovskite-based photocatalysts. Molecules 19(12):19995–20022
75. Karamian E, Sharifnia S (2018) Enhanced visible light photocatalytic activity of $BiFeO_3$–ZnO pn heterojunction for CO_2 reduction. J Mater Sci Eng B 238–239:142–148
76. Khaliullin SM, Zhuravlev V, Bamburov V (2017) Solution-combustion synthesis of $MZrO_3$ zirconates (M = Ca, Sr, Ba) in open reactor: thermodynamic analysis and experiment. Int J Self Propag High Temp Synth 26(2):93–101
77. Khan MM, Ansari SA, Pradhan D, Ansari MO, Han DH, Lee J, Cho MH (2014) Band gap engineered TiO_2 nanoparticles for visible light induced photoelectrochemical and photocatalytic studies. J Mater Chem A 2:637–644
78. Khorrami GH, Kompany A, Zak AK (2015) Structural and optical properties of (K, Na) NbO_3 nanoparticles synthesized by a modified sol–gel method using starch media. Adv Powder Technol 26(1):113–118
79. Kong J, Yang T, Rui Z, Ji H (2019) Perovskite-based photocatalysts for organic contaminants removal: current status and future perspectives. Catal Today 327:47–63
80. Kong X, Guo Z, Zeng C, Huang J, Cao L, Li L, Yin L, Wen P, Feng Q, Xu Z (2015) Soft chemical in situ synthesis, formation mechanism and electrochemical performances of 1D bead-like $AgVO_3$ nanoarchitectures. J Mater Chem A 3(35):18127–18135
81. Konta R, Kato H, Kobayashi H, Kudo A (2003) Photophysical properties and photocatalytic activities under visible light irradiation of silver vanadates. Phys Chem Chem Phys 5 (14):3061–3065
82. Kostopoulou A, Brintakis K, Nasikas NK, Stratakis E (2019) Perovskite nanocrystals for energy conversion and storage. Nanophotonics 8(10):1607–1640
83. Kou J, Lu C, Wang J, Chen Y, Xu Z, Varma RS (2017) Selectivity enhancement in heterogeneous photocatalytic transformations. Chem Rev 117:1445–1514
84. Krukowska A, Trykowski G, Lisowski W, Klimczuk T, Winiarski MJ, Zaleska-Medynska A (2018) Monometallic nanoparticles decorated and rare earth ions doped $KTaO_3/K_2Ta_2O_6$ photocatalysts with enhanced pollutant decomposition and improved H_2 generation. J Catal 364:371–381
85. Kurumisawa Y, Higashino T, Nimura S, Tsuji Y, Iiyama H, Imahori H (2019) Renaissance of fused porphyrins: substituted methylene-bridged thiophene-fused strategy for high-performance dye-sensitized solar cells. J Am Chem Soc 141:9910–9919

86. Kusiak-Nejman E, Morawski AW (2019) TiO_2/graphene-based nanocomposites for water treatment: a brief overview of charge carrier transfer, antimicrobial and photocatalytic performance. Appl Catal B Environ 253:179–186
87. Kwak BS, Kang M (2015) Photocatalytic reduction of CO_2 with H_2O using perovskite Ca x Tiy O_3. Appl Surf Sci 337:138–144
88. Lee SH, Kim H-J, Nam JW, Jung H, Kang SK, Lee K-Y (2004) Preparation of $LaCoO_3$ with high surface area for catalytic combustion by spray-freezing/freeze-drying method. Studies in surface science and catalysis, pp 463–468. Elsevier
89. Lettmann C, Hildenbrand K, Kisch H, Macyk W, Maier WF (2001) Visible light photodegradation of 4-chlorophenol with a coke-containing titanium dioxide photocatalyst. Appl Catal B Environ 32:215–227
90. Li G, Wang W, Yang N, Zhang W (2011) Composition dependence of $AgSbO_3$/$NaNbO_3$ composite on surface photovoltaic and visible-light photocatalytic properties. Appl Phys A 103(1):251–256
91. Li G, Yang W, Gao S, Shen Q, Xue J, Chen K, Li Q (2021) Creation of rich oxygen vacancies in bismuth molybdate nanosheets to boost the photocatalytic nitrogen fixation performance under visible light illumination. Chem Eng J 404:
92. Li Y, Yao S, Wen W, Xue L, Yan Y (2010) Sol–gel combustion synthesis and visible-light-driven photocatalytic property of perovskite $LaNiO_3$. J Alloy Compd 491(1–2):560–564
93. Li Y, Zhao J, Zhang G, Zhang L, Ding S, Shang E, Xia X (2019) Visible-light-driven photocatalytic disinfection mechanism of Pb-$BiFeO_3$/rGO photocatalyst. Water Res 161:251–261
94. Li J, Xu L, Wang T, Song J, Chen J, Xue J, Dong Y (2016) 50-Fold EQE improvement up to 6.27% of solution-processed all-inorganic perovskite $CsPbBr_3$ QLEDs via surface ligand density control. Adv Mater 29
95. Liqiang J, Yichun Q, Baiqi W, Shudan L, Baojiang J, Libin Y, Wei F, Honggang F, Jiazhong S (2006) Review of photoluminescence performance of nano-sized semiconductor materials and its relationships with photocatalytic activity. Sol Energy Mater Sol Cells 90:1773–1787
96. Liu J, Chen S, Liu Q, Zhu Y, Zhang J (2013) Correlation of crystal structures and electronic structures with visible light photocatalytic properties of $NaBiO_3$. Chem Phys Lett 572:101–105
97. Liu M, Jing D, Zhou Z, Guo L (2013) Twin-induced one-dimensional homojunctions yield high quantum efficiency for solar hydrogen generation. Nat Commun 4:2278
98. Liu X, Lv J, Wang S, Li X, Lang J, Su Y, Chai Z, Wang X (2015) A novel contractive effect of $KTaO_3$ nanocrystals via La^{3+} doping and an enhanced photocatalytic performance. J Alloy Compd 622:894–901
99. Liu F, Shi R, Wang Z, Weng Y, Chen Y (2019) Direct Z-scheme hetero-phase junction of black/red phosphorus for photocatalytic water splitting. Angew Chem Int Ed 58:11791
100. Liu X, Sohlberg K (2014) Theoretical calculations on layered perovskites: implications for photocatalysis. Complex Metals 1(1):103–121
101. Liu G, Wang L, Yang HG, Cheng HM, Lu GQ (2010) Titania-based photocatalysts-crystal growth, doping and heterostructuring. J Mater Chem 20:831–843
102. Liu Y, Xiao C, Li Z, Xie Y (2016) Vacancy engineering for tuning electron and phonon structures of two-dimensional materials. Adv Energy Mater 6(23):1600436
103. Liu L, Jiang Y, Zhao H, Chen J, Cheng J, Yang K et al (2016) Engineering coexposed {001} and {101} facets in oxygen-deficient TiO_2 nanocrystals for enhanced CO_2 photoreduction under visible light. ACS Catal 6(2):1097–1108
104. Low J, Yu J, Jaroniec M, Wageh S, Al-Ghamdi AA (2017) Heterojunction photocatalysts. Adv Mater 29(20):1601694
105. Lu L, Ni S, Liu G, Xu X (2017) Structural dependence of photocatalytic hydrogen production over La/Cr co-doped perovskite compound $ATiO_3$ (A = Ca, Sr and Ba). Int J Hydrogen Energy 42:23539–23547

106. Luo J (2014) Water photolysis at 12.3% efficiency via perovskite photovoltaics and Earth-abundant catalysts. Science 345:1593–1596
107. Luo C, Zhao J, Li Y, Zhao W, Zeng Y, Wang C (2018) Photocatalytic CO_2 reduction over $SrTiO_3$: correlation between surface structure and activity. Appl Surf Sci 447:627–635
108. Ly T, Wen J, Marks LD (2018) Kinetic growth regimes of hydrothermally synthesized potassium tantalate nanoparticles. Nano Lett 18:5186–5191
109. Maeda K (2014) Rhodium-doped barium titanate perovskite as a stable p-type semiconductor photocatalyst for hydrogen evolution under visible light. ACS Appl Mater Interfaces 6(3):2167–2173
110. Mai L, Xu L, Gao Q, Han C, Hu B, Pi Y (2010) Single β-$AgVO_3$ nanowire H_2S sensor. Nano Lett 10(7):2604–2608
111. Marschall R, Wang L (2014) Non-metal doping of transition metal oxides for visible-light photocatalysis. Catal Today 225:111–135
112. Mashuri SIS, Ibrahim ML, Kasim MF, Mastuli MS, Rashid U, Abdullah AH, Islam A, Asikin-Mijan N, Tan YH, Mansir N, Kaus NHM, Hin T-YY (2020) Photocatalysis for organic wastewater treatment: from the basis to current challenges for society. Catalysts 10 (11):1260
113. Mathies F, Unger E, Universität H, Physik I, Chemie I, Adlershof I, Zentrum H, Straße BT (2020) Advances in inkjet-printed metal-halide perovskitephotovoltaic and optoelectronic devices florian. Energy Technol 8
114. Matsuoka M, Kitano M, Takeuchi M, Tsujimaru K, Anpo M, Thomas JM (2007) Photocatalysis for new energy production recent advances in photocatalytic water splitting reactions for hydrogen production. Catal Today 122:51–61
115. Michel CR, Lopez-Alvarez MA, Martínez-Preciado AH, Carbajal-Arízaga GG (2019) Novel UV sensing and photocatalytic properties of $DyCoO_3$. J Sens 2019
116. Min KS, Kumar RS, Lee JH, Kim KS, Lee SG, Son YA (2019) Synthesis of new TiO_2/porphyrin-based composites and photocatalytic studies on methylene blue degradation. Dyes Pigm 160:37–47
117. Moniruddin M, Afroz K, Shabdan Y, Bizri B, Nuraje N (2017) Hierarchically 3D assembled strontium titanate nanomaterials for water splitting application. Appl Surf Sci 419:886–892
118. Moniruddin M, Ilyassov B, Zhao X, Smith E, Serikov T, Ibrayev N, Asmatulu R, Nuraje N (2018) Recent progress on perovskite materials in photovoltaic and water splitting applications. Mater Today Energy 7:246–259
119. Nundy S, Ghosh A, Mallick TK (2020) Hydrophilic and superhydrophilic self-cleaning coatings by morphologically varying ZnO microstructures for photovoltaic and glazing applications. OCS Omega 5:1033–1039
120. Nuraje N, Asmatulu R, Kudaibergenov S (2012) Metal oxide-based functional materials for solar energy conversion: a review. Curr Inorg Chem 2(2):124–146
121. Ola O, Maroto-Valer MM (2015) Review of material design and reactor engineering on TiO_2 photocatalysis for CO_2 reduction. J Photochem Photobiol C Photochem Rev 24:16–42
122. Onishi H (2019) Sodium tantalate photocatalysts doped with metal cations: why are they active for water splitting? Chemsuschem 12(9):1825–1834
123. Ou Q, Bao X, Zhang Y, Shao H, Xing G, Li X (2019) Band structure engineering in metal halide perovskite nanostructures for optoelectronic applications. Nano Mater Sci 1:268–287
124. Paramanik L, Reddy KH, Sultana S, Parida K (2018) Architecture of biperovskite-based $LaCrO_3$/$PbTiO_3$ p–n heterojunction with a strong interface for enhanced charge anti-recombination process and visible light-induced photocatalytic reactions. Inorg Chem 57(24):15133–15148
125. Paramanik L, Parida K (2020) Efficient perovskite titanate photocatalysts for oxygen evolution reactions. Mater Today: Proc
126. Park S, Chang WJ, Lee CW, Park S, Ahn HY, Nam KT (2017) Photocatalytic hydrogen generation from hydriodic acid using methylammonium lead iodide in dynamic equilibrium with aqueous solution. Nat Energy 2:1–8

127. Park B, Philippe B, Zhang X, Rensmo H, Boschloo G, Johansson EMJ (2015) Bismuth based hybrid perovskites $A_3Bi_2I_9$ (a: methylammonium or cesium) for solar cell application. Adv Mater 27:6806–6813
128. Ran C, Xu J, Gao W, Huang C, Dou S (2018) Defects in metal triiodide perovskite materials towards high-performance solar cells: origin, impact, characterization, and engineering. Chem Soc Rev 47:4581–4610
129. Rao MP, Nandhini VP, Wu JJ, Syed A, Ameen F, Anandan S (2018) Synthesis of N-doped potassium tantalate perovskite material for environmental applications. J Solid State Chem 258:647–655
130. Ren Z, Wang N, Wei P, Cui M, Li X, Qin C (2020) Ultraviolet-ozone modification on TiO_2 surface to promote both efficiency and stability of low-temperature planar perovskite solar cells. Chem Eng J 393:124731
131. Ren P, Song M, Lee J, Zheng J, Li D (2019) Edge dislocations induce improved photocatalytic efficiency of colored TiO_2. Adv Mater Inter 1901121
132. Rokesh K, Sakar M, Do TO (2020) Calcium bismuthate ($CaBiO_3$): a potential sunlight-driven perovskite photocatalyst for the degradation of emerging pharmaceutical contaminants. ChemPhotoChem
133. Roy P, Sinha NK, Tiwari T, Khare A (2020) A review on perovskite solar cells: evolution of architecture, fabrication techniques, commercialization issues and status. Sol Energy 198:665–668
134. Ruzimuradov O, Hojamberdiev M, Fasel C, Riedel R (2017) Fabrication of lanthanum and nitrogen—Co-doped $SrTiO_3$–TiO_2 heterostructured macroporous monolithic materials for photocatalytic degradation of organic dyes under visible light. J Alloys Compd 699:144–150
135. Safari S, Ahmadian SMS, Amani-Ghadim AR (2020) Visible light photocatalytic activity enhancing of $MTiO_3$ perovskites by M cation (M = Co, Cu, and Ni) substitution and Gadolinium doping. J Photochem Photobiol, A 394:112461
136. Samsudin EM, Abd Hamid SB (2017) Effect of band gap engineering in anionic-doped TiO_2 photocatalyst. Appl Surf Sci 391:326–336
137. Satar NSA, Adnan R, Lee HL, Hall SR, Kobayashi T, Kassim MHM, Kaus NHM (2019) Facile green synthesis of ytrium-doped $BiFeO_3$ with highly efficient photocatalytic degradation towards methylene blue. Ceram Int 45(13):15964–15973
138. Satar NSA, Aziz AW, Yaakob MK, Yahya MZA, OH Hassan OH, Kudin TIT, Mohd Kaus NH (2016) Experimental and first-principles investigations of lattice strain effect on electronic and optical properties of biotemplated $BiFeO_3$ nanoparticles. J Phys Chem C 120 (45):26012–26020
139. Schmidt R, Prado-Gonjal J, Ávila D, Amador U, Morán E (2014) Electron microscopy of microwave-synthesized rare-earth chromites. arXiv:14095607
140. Shamblin J, Heres M, Zhou H, Sangoro J, Lang M, Neuefeind J, Alonso J, Johnston S (2018) Experimental evidence for bipolaron condensation as a mechanism for the metal-insulator transition in rare-earth nickelates. Nat Commun 9(1):1–7
141. Shi Z, Guo J, Chen Y, Li Q, Pan Y, Zhang H, Xia Y, Huang W (2017) Lead-free organic–inorganic hybrid perovskites for photovoltaic applications: recent advances and perspectives. Adv Mater 29(16):1605005
142. Shi H, Wang T, Chen J, Zhu C, Ye J, Zou Z (2011) Photoreduction of carbon dioxide over $NaNbO_3$ nanostructured photocatalysts. Catal Lett 141(4):525–530
143. Shi R, Waterhouse GI, Zhang T (2017) Recent progress in photocatalytic CO_2 reduction over perovskite oxides. Solar Rrl 1(11):1700126
144. Shi R, Zhao Y, Waterhouse G, Zhang S, Zhang T (2019) Defect engineering in photocatalytic nitrogen fixation. ACS Catal 9:9739–9750
145. Shi H, Fan J, Zhao Y, Hu X, Zhang X, Tang Z (2020) Visible light driven $CuBi_2O_4$/Bi_2MoO_6 p-n heterojunction with enhanced photocatalytic inactivation of *E. coli* and mechanism insight. J Hazard Mater 381:121006
146. Shintaro I, Namhoon K, Elif E, Sakae T, Tatsumi I (2015) Photocatalytic reaction centers in two-dimensional titanium oxide crystals. J Am Chem Soc 137:239

147. Si H, Liao Q, Zhang Z, Li Y, Yang X, Zhang G, Kang Z, Zhang Y (2016) An innovative design of perovskite solar cells with Al_2O_3 inserting at ZnO/perovskite interface for improving the performance and stability. Nano Energy 22:223–231
148. Singh J, Uma S (2009) Efficient photocatalytic degradation of organic compounds by ilmenite $AgSbO_3$ under visible and UV light irradiation. J Phys Chem C 113(28):12483–12488
149. Situmeang RTM (2019) Pectins as emulsifying agent on the preparation, characterization, and photocatalysis of nano-$LaCrO_3$. Pectins-extraction, purification, characterization and applications. IntechOpen
150. Sivakumar V, Suresh R, Giribabu K, Narayanan V (2015) $AgVO_3$ nanorods: synthesis, characterization and visible light photocatalytic activity. Solid State Sci 39:34–39
151. Su T-M, Qin Z-Z, Ji H-B, Jiang Y-X, Huang G (2016) Recent advances in the photocatalytic reduction of carbon dioxide. Environ Chem Lett 14(1):99–112
152. Suk J, Gyu H, Sung J (2012) Heterojunction semiconductors: a strategy to develop efficient photocatalytic materials for visible light water splitting. Catal Today 185:270–277
153. Sun J, Chen G, Li Y, Jin R, Wang Q, Pei J (2011) Novel (Na, K) TaO_3 single crystal nanocubes: molten salt synthesis, invariable energy level doping and excellent photocatalytic performance. Energy Environ Sci 4(10):4052–4060
154. Sun WJ, Li J, Mele G, Zhang ZQ, Zhang FX (2013) Enhanced photocatalytic degradation of rhodamine B by surface modification of ZnO with copper (II) porphyrin under both UV–vis and visible light irradiation. J Mol Catal A: Chem 366:84–91
155. Sun L, Li R, Zhan W, Wang F, Zhuang Y, Wang X, Han X (2019) Rationally designed double-shell dodecahedral microreactors with efficient photoelectron transfer: N-Doped-C-Encapsulated ultrafine In_2O_3 nanoparticles. Chem A Eur J 25:3053–3060
156. Tachikawa T, Tojo S, Kawai K, Endo M, Fujitsuka M, Ohno T, Nishijima K, Miyamoto Z, Majima T (2004) Photocatalytic oxidation reactivity of holes in the sulfur- and carbon-doped TiO_2 powders studied by time-resolved di use reflectance spectroscopy. J Phys Chem B 108:19299–19306
157. Takagi K, Makimoto T, Hiraiwa H, Negishi T (2001) Photocatalytic, antifogging mirror. J Vac Sci Technol, A 19:2931
158. Takata Y, Hidaka S, Cao JM, Nakamura T, Yamamoto H, Masuda M, Ito T (2005) Effect of surface wettability on boiling and evaporation. Energy 30:209–220
159. Takei T, Haramoto R, Dong Q, Kumada N, Yonesaki Y, Kinomura N, Mano T, Nishimoto S, Kameshima Y, Miyake M (2011) Photocatalytic activities of various pentavalent bismuthates under visible light irradiation. J Solid State Chem 184(8):2017–2022
160. Tan Y, Shu Z, Zhou J, Li T, Wang W, Zhao Z (2018) One-step synthesis of nanostructured g-C_3N_4/TiO_2 composite for highly enhanced visible-light photocatalytic H_2 evolution. Appl Catal B 230:260–268
161. Tanaka H, Misono M (2001) Advances in designing perovskite catalysts. Curr Opin Solid State Mater Sci 5(5):381–387
162. Tang P, Tong Y, Chen H, Cao F, Pan G (2013) Microwave-assisted synthesis of nanoparticulate perovskite $LaFeO_3$ as a high active visible-light photocatalyst. Curr Appl Phys 13(2):340–343
163. Taylor P, Yunus IS, Kurniawan A, Adityawarman D, Indarto A (2012) Nanotechnologies in water and air pollution treatment. Environ Technol Rev 1:136–148
164. Teh YW, Chee MK, Kong XY, Yong S-T, Chai S-P (2020) An insight into perovskite-based photocatalysts for artificial photosynthesis. Sustain Energy Fuels 4(3):973–984
165. Teramura K, Okuoka S-I, Tsuneoka H, Shishido T, Tanaka T (2010) Photocatalytic reduction of CO_2 using H_2 as reductant over $ATaO_3$ photocatalysts (A = Li, Na, K). Appl Catal B 96:565–568
166. Terranova U, Viñes F, de Leeuw NH, Illas F (2020) Mechanisms of carbon dioxide reduction on strontium titanate perovskites. J Mater Chem A 8(18):9392–9398

167. Vidal K, Morán-Ruiz A, Larrañaga A, Porras-Vázquez J, Slater P, Arriortua M (2015) Characterization of LaNi0. 6Fe0. 4O3 perovskite synthesized by glycine-nitrate combustion method. Solid State Ionics 269:24–29
168. Wang X, Bai L, Liu H, Yu X, Yin Y, Gao CA (2018) Unique disintegration-reassembly route to mesoporous titania nanocrystalline hollow spheres with enhanced photocatalytic activity. Adv Funct Mater 28:1–8
169. Wang Y, Cheng H-P (2013) Oxygen reduction activity on perovskite oxide surfaces: a comparative first-principles study of $LaMnO_3$, $LaFeO_3$, and $LaCrO_3$. J Phys Chem C 117 (5):2106–2112
170. Wang F, DiValentin C, Pacchioni G (2012) Rational band gap engineering of WO_3 photocatalyst for visible light water splitting. Chem Cat Chem 4:476–478
171. Wang S, Hai X, Ding X, Chang K, Xiang Y, Meng X, Yang Z, Chen H, Ye J (2017) Light-switchable oxygen vacancies in ultrafine Bi_5O_7Br nanotubes for boosting solar-driven nitrogen fixation in pure water. Adv Mater 29:1701774
172. Wang F, He X, Sun L, Chen J, Wang X, Xu J, Han X (2018) Engineering an N-doped TiO_2@N-doped C butterfly-like nanostructure with long-lived photo-generated carriers for efficient photocatalytic selective amine oxidation. J Mater Chem A 6:2091–2099
173. Wang N, Kong D, He H (2011) Solvothermal synthesis of strontium titanate nanocrystallines from metatitanic acid and photocatalytic activities. Powder Technol 207(1–3):470–473
174. Wang R, Ni S, Liu G, Xu X (2018) Hollow $CaTiO_3$ cubes modified by La/Cr co-doping for efficient photocatalytic hydrogen production. Appl Catal B 225:139–147
175. Wang Z, Su B, Xu J, Hou Y, Ding Z (2020) Direct Z-scheme $ZnIn_2S4/LaNiO_3$ nanohybrid with enhanced photocatalytic performance for H_2 evolution. Int J Hydrogen Energy 45 (7):4113–4121
176. Wang H, Yuan X, Wu Y, Zeng G, Tu W, Sheng C, Deng Y, Chen F, Chew JW (2017) Plasmonic Bi nanoparticles and BiOCl sheets as cocatalyst deposited on perovskite-type $ZnSn(OH)_6$ microparticle with facet-oriented polyhedron for improved visible-light-driven photocatalysis. Appl Catal B 209:543–553
177. Wang F, Zhang J, Yuan P, Yan Q, Zhang P (2000) Magnetic and transport properties of vanadate $PrVO_3$. J Phys: Condens Matter 12(13):3037
178. Wei S, Xu X (2018) Boosting photocatalytic water oxidation reactions over strontium tantalum oxynitride by structural laminations. Appl Catal B 228:10–18
179. Weng D, Lei C, Wu TT, Sun R, Shen M, Lu Y (2015) Spontaneous and continuous anti-virus disinfection from nonstoichiometric perovskite-type lanthanum manganese oxide. Prog Nat Sci 25(3):191–196
180. Wu X, Wang C, Wei Y, Xiong J, Zhao Y, Zhao Z, Liu J, Li J (2019) Multifunctional photocatalysts of Pt-decorated 3DOM perovskite-type $SrTiO_3$ with enhanced CO_2 adsorption and photoelectron enrichment for selective CO_2 reduction with H_2O to CH_4. J Catal 377:309–321
181. Xie K, Umezawa N, Zhang N, Reunchan P, Zhang Y, Ye J (2011) Self-doped $SrTiO_3$–δ photocatalyst with enhanced activity for artificial photosynthesis under visible light. Energy Environ Sci 4:4211–4219
182. Xu J, Hu C, Xi Y, Wan B, Zhang C, Zhang Y (2012) Synthesis and visible light photocatalytic activity of β-$AgVO_3$ nanowires. Solid State Sci 14(4):535–539
183. Xu C, Ravi Anusuyadevi P, Aymonier C, Luque R, Marre S (2019) Nanostructured materials for photocatalysis. Chem Soc Rev 48:3868–3902
184. Xu D, Shi W, Song C, Chen M, Yang S, Fan W, Chen B (2016) In-situ synthesis and enhanced photocatalytic activity of visible-light-driven plasmonic $Ag/AgCl/NaTaO_3$ nanocubes photocatalysts. Appl Catal B 191:228–234
185. Yan Y, Gu J, Zeitler EL, Bocarsly AB (2015) Photoelectrocatalytic reduction of carbon dioxide. In: Peter S, Elsje AQ, Katy A (eds) Carbon dioxide utilisation. Elsevier, Oxford, pp 211–233

186. Yang Y, Kang L, Li H (2019) Enhancement of photocatalytic hydrogen production of $BiFeO_3$ by Gd^{3+} doping. Ceram Int 45:8017–8022
187. Yao J-S, Ge J, Han B-N, Wang K-H, Yao H-B, Yu H-L, Li J-H, Zhu B-S, Song J-Z, Chen C (2018) Ce^{3+} -doping to modulate photoluminescence kinetics for efficient $CsPbBr_3$ nanocrystals based light-emitting diodes. J Am Chem Soc 140(10):3626–3634
188. Yao S, Zheng R, Li R, Chen Y, Zhou X, Luo J (2019) Construction of Z-scheme $LaNiO_3$/SnS_2 composite for boosting visible light photodegradation of tetracycline. J Taiwan Inst Chem Eng 100:186–193
189. Yu ZB, Xie YP, Liu G, Lu GQ, Ma XL, Cheng HM (2013) Self-assembled CdS/Au/ZnO heterostructure induced by surface polar charges for efficient photocatalytic hydrogen evolution. J Mater Chem A 1:2773–2776
190. Yu J, Low J, Xiao W, Zhou P, Jaroniec, M (2014) Enhanced photocatalytic CO_2-reduction activity of anatase TiO_2 by coexposed {001} and {101} facets. J Am Chem Soc 136 (25):8839–8842. https://doi.org/10.1021/ja5044787
191. Zeng Z, Xu Y, Zhang Z, Gao Z, Luo M, Yin Z, Zhang C, Xu J, Huang B, Luo F (2020) Rare-earth-containing perovskite nanomaterials: design, synthesis, properties and applications. Chem Soc Rev 49(4):1109–1143
192. Zhang N, Gao C, Xiong Y (2019) Defect engineering: a versatile tool for tuning the activation of key molecules in photocatalytic reactions. J Energy Chem 37:43
193. Zhang G, Liu G, Wang L, Irvine JTS (2016) Inorganic perovskite photocatalysts for solar energy utilization. Chem Soc Rev 45:5951–5984
194. Zhang G, Liu G, Wang L, Irvine JT (2016) Inorganic perovskite photocatalysts for solar energy utilization. Chem Soc Rev 45(21):5951–5984
195. Zhang G, Sewell CD, Zhang P, Mi H, Lin Z (2020) Nanostructured photocatalysts for nitrogen fixation. Nano Energy 71:104645
196. Zhang J, Wang A, Zhao W, Li C, Chen X, Wang Y, Zhu W, Zhong Q (2018) Influence of metal-porphyrins on the photocatalysis of graphitic carbon nitride. Dyes Pigm 153:241–247
197. Zhang H, Zhang X, Yang G, Zhou X (2018) Point defect effects on photoelectronic properties of the potential metal-free C2N photocatalysts: insight from first-principles computations. J Phys Chem C 122:5291–5302
198. Zhang S, Zhao Y, Shi R, Waterhouse G, Zhang T (2019) Photocatalytic ammonia synthesis: recent progress and future. Energy Chem 1:100013
199. Zheng Z, Huang B, Lu J, Wang Z, Qin X, Zhang X, Dai Y, Whangbo MH (2012) Hydrogenated titania: synergy of surface modification and morphology improvement for enhanced photocatalytic activity. Chem Commun 48:5733–5735
200. Zheng Z, Huang B, Qin X, Zhang X, Dai Y (2011) Facile synthesis of $SrTiO_3$ hollow microspheres built as assembly of nanocubes and their associated photocatalytic activity. J Colloid Interface Sci 358(1):68–72
201. Zhong F, Zhuang H, Gu Q, Long J (2016) Structural evolution of alkaline earth metal stannates $MSnO_3$ (M = Ca, Sr, and Ba) photocatalysts for hydrogen production. RSC Adv 6 (48):42474–42481
202. Zhong D, Liu W, Tan P, Zhu A, Liu Y, Xiong X, Pan J (2018) Insights into the synergy effect of anisotropic {001} and {230}facets of $BaTiO_3$ nanocubes sensitized with CdSe quantum dots for photocatalytic water reduction. Appl Catal B 227:1–12
203. Zhou H, Guo J, Li P, Fan T, Zhang D, Ye J (2013) Leaf-architectured 3D hierarchical artificial photosynthetic system of perovskite titanates towards CO_2 photoreduction into hydrocarbon fuels. Sci Rep 3:1667
204. Zhou W-L, Zhao Z-Y (2016) Electronic structures of efficient $MBiO_3$ (M = Li, Na, K, Ag) photocatalyst. Chin Phys B 25(3):037102
205. Zhou D, Zhou T, Tian Y, Zhu X, Tu Y (2018) Perovskite-based solar cells: materials, methods, and future perspectives. J Nanomater 1–12
206. Zhu L, Shao Z, Ye J, Zhang X, Pan X, Dai S (2016) Mesoporous $BaSnO_3$ layer based perovskite solar cells. Chem Commun 52(5):970–973

207. Zhu Y, Zhou W, Shao Z (2017) Perovskite/carbon composites: applications in oxygen electrocatalysis. Small 13(12):1603793
208. Zlotnik S, Tobaldi DM, Seabra P, Labrincha JA, Vilarinho PM (2016) Alkali niobate and tantalate perovskites as alternative photocatalysts. Chem Phys